Scientific Research Publishing

Open Journal of Modelling and Simulation, 2024, 12, 1-32
https://www.scirp.org/journal/ojmsi
ISSN Online: 2327-4026
ISSN Print: 2327-4018

Seasonal Prediction of Indian Summer Monsoon Using WRF: A Dynamical Downscaling Perspective

Manas Ranjan Mohanty[1], Uma Charan Mohanty[2]

[1]Department of Atmospheric and Oceanic Sciences, University of California, Los Angeles, USA
[2]Centre for Climate Smart Agriculture, Siksha O Anusandhan Deemed to Be University, Odisha, India
Email: manasmohanty90@gmail.com

How to cite this paper: Mohanty, M.R. and Mohanty, U.C. (2024) Seasonal Prediction of Indian Summer Monsoon Using WRF: A Dynamical Downscaling Perspective. *Open Journal of Modelling and Simulation*, **12**, 1-32.
https://doi.org/10.4236/ojmsi.2024.121001

Received: November 2, 2023
Accepted: January 12, 2024
Published: January 15, 2024

Abstract

Seasonal forecasting of the Indian summer monsoon by dynamically downscaling the CFSv2 output using a high resolution WRF model over the hindcast period of 1982-2008 has been performed in this study. The April start ensemble mean of the CFSv2 has been used to provide the initial and lateral boundary conditions for driving the WRF. The WRF model is integrated from 1st May through 1st October for each monsoon season. The analysis suggests that the WRF exhibits potential skill in improving the rainfall skill as well as the seasonal pattern and minimizes the meteorological errors as compared to the parent CFSv2 model. The rainfall pattern is simulated quite closer to the observation (IMD) in the WRF model over CFSv2 especially over the significant rainfall regions of India such as the Western Ghats and the central India. Probability distributions of the rainfall show that the rainfall is improved with the WRF. However, the WRF simulates copious amounts of rainfall over the eastern coast of India. Surface and upper air meteorological parameters show that the WRF model improves the simulation of the lower level and upper-level winds, MSLP, CAPE and PBL height. The specific humidity profiles show substantial improvement along the vertical column of the atmosphere which can be directly related to the net precipitable water. The CFSv2 underestimates the specific humidity along the vertical which is corrected by the WRF model. Over the Bay of Bengal, the WRF model overestimates the CAPE and specific humidity which may be attributed to the copious amount of rainfall along the eastern coast of India. Residual heating profiles also show that the WRF improves the thermodynamics of the atmosphere over 700 hPa and 400 hPa levels which helps in improving the rainfall simulation. Improvement in the land surface fluxes is also witnessed in the WRF model.

Keywords

Dynamical Downscaling, Regional and Mesoscale Modeling, Diabatic Heating, WRF

1. Introduction

The Indian summer monsoon covering four months of a year from June to September influences about $1/7^{th}$ of the entire world's population as well the economy associated with the Indian sub-continent. The significance of the monsoon and its prospects for early prediction have been addressed in numerous studies over the past few decades. About 80% of the annual rainfall is received during these months for which agricultural activities as well as water bodies management are largely dependent on it [1] [2]. About 8% of India's net GDP and 49% of direct/indirect employment is associated with agriculture [3]. The early prediction of the nature of a particular monsoon season is of great demand because of the large-scale dependencies of the sectors such as hydro-power, mining, irrigation, water body management, etc. on the net rainfall received during the monsoon season. Numerous studies have been carried out in the field of hydrology where the impact of rainfall at short term and seasonal scales has indicated that the rainfall has a significant control on the river networks [4] [5]. Climate change possesses a potential threat to river hydrology and the hydrological cycle in urban areas especially. Studies by Yuan *et al.* [6] over Mekong River basin have pointed out that the location of the planned dams can alter hydrological cycle and in the current scenario of climate change may hamper environmental integrity of the region.

Operational forecasting of the monsoons is largely carried out by general circulation models (GCMs) and to some extent by statistical/regression models [7]-[11]. Modern techniques have also developed a hybrid dynamical-statistical modeling framework for minimizing the errors from a dynamical model. The forecasting skill with the contemporary methods of forecasting have gained tremendous improvement by still have certain lacunae and fail to produce a skillful forecast of the most vital parameter, *i.e.* rainfall. GCMs have the hindrances in the form of coarse resolution, improper representation of the land surface, computational constraints, representation of the sub-grid scale processes, etc. [12] [13] [14] [15]. Further, systematic biases possessed by a GCM due to the internal dynamics of the model have been a source of constant errors and removal of the systematic biases along with improvement in the internal dynamics has been a broad area of research in the present time [16]. Studies to test the skill of the GCMs in simulating the seasonal rainfall at a lead time of 2 - 3 months have inferred that the models have poor temporal correlation skill with the observations [17] [18] [19]. There have been particular case studies depicting the failure of dynamical models in forecasting the summer monsoon and most of the

studies attributed to the chaotic representation of the atmosphere. The non-linearity in representing the atmosphere needs to be addressed in the dynamical models to quantify the proper behavior of the global atmospheric conditions [20] [21] [22] [23]. There have been inputs from scientists across the globe to use empirical models for removing the errors in a dynamical model and generate skillful forecast even at local scales using a hybrid dynamical-statistical framework.

The potential predictability of the monsoons is limited and lower than rest of the globe as the summer monsoon is influenced by a lot of global scale processes such as the ENSO, IOD, EQUINOO, etc. [24]. The rainfall during an active El-Nino period can cause changes to the mean seasonal rainfall and hence can alter the river hydrology thereby creating severe aricultural droughts [5]. The monsoon rainfall is largely influenced by the above-mentioned large-scale processes on a lagged time frame [25] [26] [27]. The complexities associated with the summer monsoon rainfall are mainly because of the mesoscale convective activities, land surface heterogeneities, interannual variability, etc. Recent studies have claimed that the monsoon rainfall variability has increased over the past few decades [28] [29]. There have been changes in ISM mean circulation, increased heavy rainfall events during the monsoon over the past few years [30] [31] [32]. Due to these complexities, the dynamical models struggle to simulate the rainfall variability during the monsoon seasons. Thus, despite considerable progress in predicting dynamical features of ISM variability, models still fail to simulate the mean and interannual variability of monsoon rainfall [33]. There have been attempts to improve the skill by using ensemble prediction approach, boot-strapping methods and statistical methods [34] [35]. Despite these efforts, the multi-model ensemble prediction skill is sometimes better and sometimes not noticeably better than the individual forecasts [36].

An alternative approach to improve the predictive skill can be achieved in the form of downscaling of the GCM forecasts using an RCM. RCMs have the advantage of finer grid spacing thereby having better representation of the terrain, improved representation of the sub-grid scale processes which may help in minimize the errors and improve the seasonal forecasts can be by the process of downscaling the GCMs using an RCM. Besides, RCMs have their own physical parametrization of the sub-grid scale processes which can be customized for a particular region of forecast interest. Thus, systematic biases in GCMs arising due to topography, model physics, can be addressed and reduced by the process of dynamical downscaling. The method of dynamically downscaling the GCM output using a RCM has been widely investigated by researchers for the purpose of improving the skill of seasonal prediction of the Indian summer monsoon which can be dated back to late 1990s. RCMs and mesoscale models have been used in numerous past studies and some of the models captured to simulate the mean circulation whereas other failed to even represent the mean rainfall pattern [37]-[49]. For Indian summer monsoon, the RegCM and WRF models have

been primarily and widely used over other RCMs [50] [51] [52] [53]. The RegCM is a climate model whereas the WRF is a mesoscale model but both the models have shown to possess good skill while simulating the summer monsoon. With the RCMs, the avenue for improving the GCM forecasts have opened up a chance for more skillful and target-oriented forecast [54] [55]. However not all RCMs do not have potential skill to simulate the complex climatic features [56]. Some researchers also propose that the forecasts can be improved by statistical downscaling as well.

RCMs have their own limitations in the form of physical process parametrization, choice and position of boundary conditions, domain size and grid spacing selection to name a few [57] [58]. Combination of suitable parametrization schemes, frequent update of the boundary conditions, positioning of the RCM boundary with minimum input errors from the GCM, time period of simulation has to be taken cate of while using a RCM to get the maximum utility of a RCM. Continuous re-initialization of a RCM at specific time and lateral boundary has been used for several downscaling experiments to reduce the errors in a RCM. Maurya *et al.*, [47] made a point that the grid spacing can be made finer but up to a certain extent beyond which the skill deteriorates further. Mohanty & Mohanty [51] compared the skill of two RCMs, RegCM4 and WRF4 in simulating the Indian summer monsoon using CFSv2 initial conditions and found that both the RCMs improved the rainfall pattern and intensities over the parent GCM. Both the models possessed patches of dry and wet bias. Similarly, the surface and upper air parameters were improved while using the RCMs. Overall, they concluded that the WRF presented better skill in simulating the rainfall as well as significant meteorological parameters for normal as well as extreme monsoon seasons.

This study is aimed at downscaling high resolution CFSv2 (~38 km) output using WRF4 model. A brief description of the data used, and the methodology followed is explained in Section 2. The results and discussions are presented in Section 3 whereas the conclusion is presented in Section 4.

2. Data and Methodology

For downscaling the CFSv2 output, the WRF version 4 is used as the RCM. WRF is one of the widely used mesoscale models serving both research and operational forecasting purposes [59]. The model configuration and the parameterization schemes used in the downscaling experiments have been shown briefly in **Table 1**.

The CFSv2 output at T382 spectral resolution (~38 km) from the 9-month runs are used as the initial and lateral boundary conditions for the WRF model. The CFSv2 ensembles from the month of April initialized at 5th, 10th, 15th, 20th and 25th of April at 00UTC are averaged out to provide the 6-hourly Initial and Boundary Conditions (ICBC). The WRF model is initialized from 1st of May through 1st of October, and the model analysis are done for the Indian summer monsoon (JJAS) months. The month of May is considered as the spin up time

Table 1. WRF4 configuration used in the present study.

Model domain	5˚S - 40˚N; 55˚E - 110˚E
Initial Condition (CFSv2)	Ensemble mean of 5th, 10th, 15th, 20th, 26th April 00UTC
Simulation period	1st May to 1st October (Each Year)
No. of vertical levels	35 σ levels
Horizontal Resolution	15 km
Central longitude and latitude	79˚E and 21˚N
Dynamical core	Hydrostatic (ARW)
Map-projection	Rotated Mercator
Cumulus convection scheme	Kain-Fritsch (new Eta) scheme
Radiation Scheme	RRTM
Boundary layer scheme	YSU scheme
Microphysics scheme	WRF Single-Moment (WSM) 5-class
Land Surface Physics	Noah land surface model

for the model and is truncated from the analysis. For the analysis, the rainfall is first verified based on the eyeball method followed by some significant statistical verification scores. The rainfall simulated is verified with the IMD gridded daily rainfall data set at $0.25^0 \times 0.25^0$ [60] whereas the upper air parameters are verified with the ERA5 data sets at $0.25^0 \times 0.25^0$ spatial resolutions [61]. The model is simulated for 27 consecutive monsoon seasons over the period of 1982-2008, of which 17 are normal, 5 are excess and 5 are deficit monsoon seasons. Along with the monsoon climatology, the model is evaluated for the composites of excess, normal and deficit monsoon seasons. The horizontal resolution of the WRF is confined at 15 km.

Mean Percentage Error (MPE):

The formula for computing the MPE is

$$\text{MPE} = \frac{100}{n}\sum_{t=1}^{n}\frac{O-F}{O}$$

where O = Observed rainfall.

F = Forecasted ranfall.

n = number of years.

The MPE is thus based on the actual forecast errors rather than absolute forecast errors.

Phase Synchronizing Events (PSE):

The number of simulated rainfall events lying on the same side of the rainfall anomaly to that of the observed anomaly is said to be in the same phase to that of the observed. The total number of years in the CFSv2 and WRF that possess the same sign to that of the IMD rainfall anomaly are calculated and expressed in percentage.

3. Results and Discussions

The verification of the WRF in downscaling the CFSv2 output has been carried out in the following sections. The verification is divided into two sections where the 1st section is aimed at verifying the rainfall comprehensively and the 2nd section looks into the skill of the models in simulating the monsoon climatic features and the possible reasons for the discrepancies in rainfall simulation.

3.1. Rainfall

The rainfall from the CFSv2 reforecasts along with the downscaled rainfall from WRF simulations are compared on the climatological scale of 27 years and with the composite excess, normal and deficit years. Figure 1 represents the rainfall climatology along with the composites as observed and as simulated by the CFSv2 and WRF. The rainfall as observed over the 27 years shows that the rainfall is quite heterogeneous over India ranging from 100 - 2500 mm during the

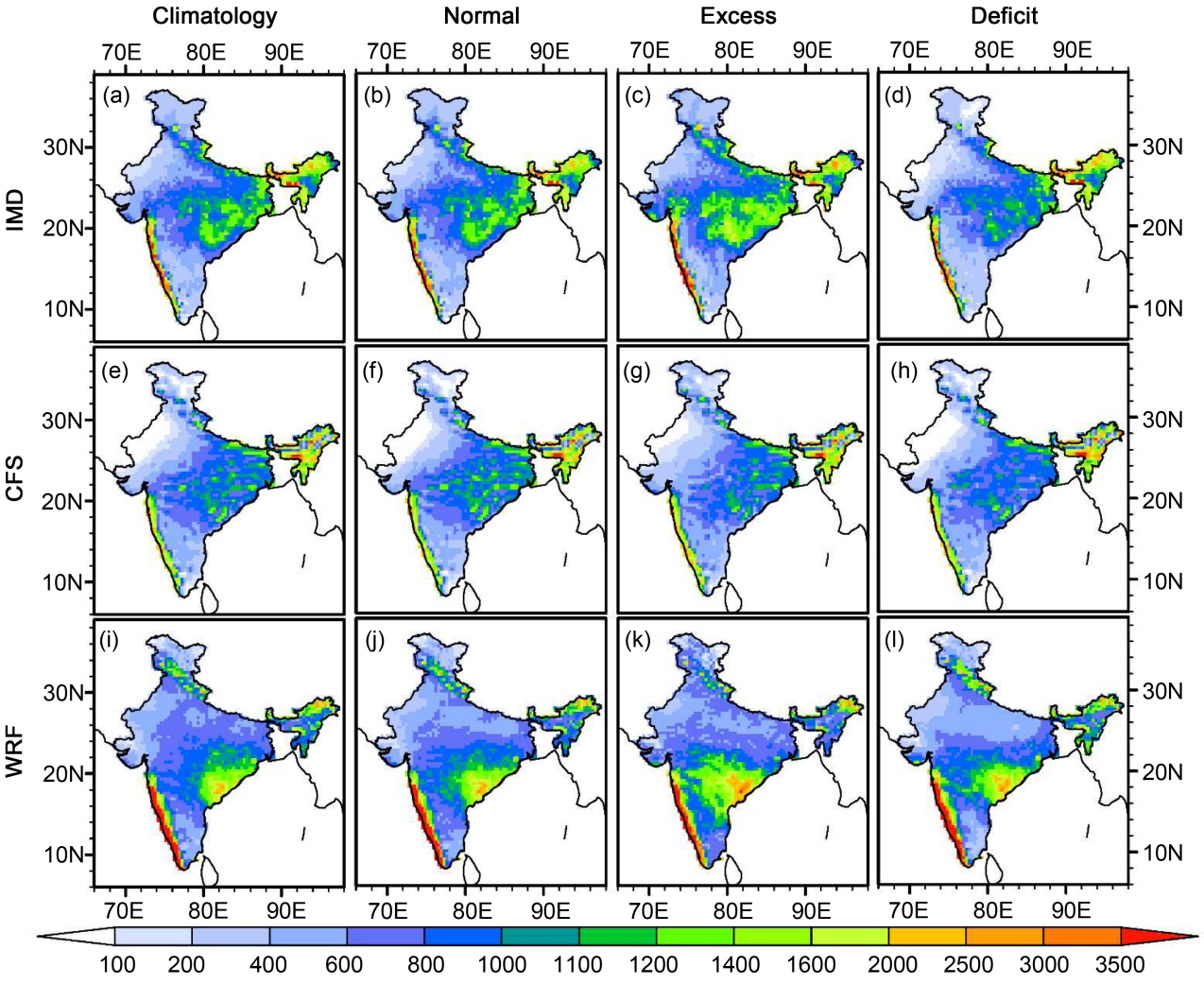

Figure 1. Mean seasonal (JJAS) rainfall (in mm) averaged (a) over the hindcast period of 1982-2008 and that of the composite (b) normal (c) excess and (d) deficit monsoon seasons as observed in IMD. Panels (e)-(h) and (i)-(l) are same as (a)-(d) but as simulated by CFSv2 and WRF respectively.

JJAS months. Maximum rainfall regions can be witnessed over the Western Ghats, northeastern India followed by central India and the Gangetic plains. During the monsoon seasons, the rainfall is very scanty over the northwestern India as well as the south peninsular India. The analysis of composite monsoon seasons shows that the rainfall is quite discrepant between the excess, normal and deficit seasons. During the excess monsoon seasons, the rainfall is mostly excess over the central India region which is also analogous in the deficit monsoon seasons where there is very less rainfall over the states of Odisha, Jharkhand, Madhya Pradesh, Bihar. The rainfall variability between the seasons can be clearly identified from the composite years and this supports the fact that small variability in rainfall can create havocs in the rain-fed agricultural regions of India. The rainfall during the deficit seasons lies between the range 600 - 1400 mm as compared to 800 - 2000 mm in the excess monsoon season. On comparing the observed rainfall with the model simulated rainfall, the CFSv2 simulates very less amount of rainfall over the core monsoon region. The rainfall in CFSv2 is underestimated in the Western Ghats as well as over the central India region. Another peculiar feature of the rainfall simulated by the CFSv2 is that the rainfall over northwestern India is very less and is not all well simulated. The dry bias in this region is too high. Over the central India region, the rainfall simulated by CFSv2 shows patches of dry and wet regions which may be arising due to the representation of terrain in the model. The excess monsoon seasons are not quite well captured by the CFSv2. However, during the deficit monsoon season, the model has a closer rainfall pattern to that of the observed data set. On the other hand, downscaling the CFSv2 using WRF has better performance in terms of reproducing the rainfall pattern during the monsoon seasons. Maximum rainfall patches over the Western Ghats, central India and northeast India are reproduced by the WRF model. Over maximum regions of India, the WRF model has closer pattern to that of the IMD rainfall dataset. Over the northeastern India, the WRF simulates lesser rainfall than the CFSv2 as well as IMD. CFSv2 has better predictability of rainfall over the hilly regions of northeast which is missed with the WRF model. Along with that, the net simulated monsoon rainfall for the composites of excess, normal and deficit seasons have closer relationship with the observed data set. During the excess monsoon season, the rainfall is higher than the normal and deficit monsoon seasons. However, the rainfall over the Western Ghats is overestimated in the WRF model. It may be arising because of the orography of this region. Fine representation of the Western Ghats may be leading to orographic lifting of air parcel thereby influencing the static stability of the parcel and ultimately leading to excessive rainfall. The rainfall ranges between 800 - 1800 mm/400 - 1000 mm/600 - 1600 mm in the central India region with IMD/CFSv2/WRF respectively. Over the Western Ghats, the rainfall is 1200 - 3000 mm/1000 - 1600 mm/1400 - 3500 mm with the IMD/CFSv2/WRF models respectively.

The mean rainfall bias between the CFSv2/WRF and IMD for all the years of study along with the composite monsoon seasons is shown in **Figure 2**. The

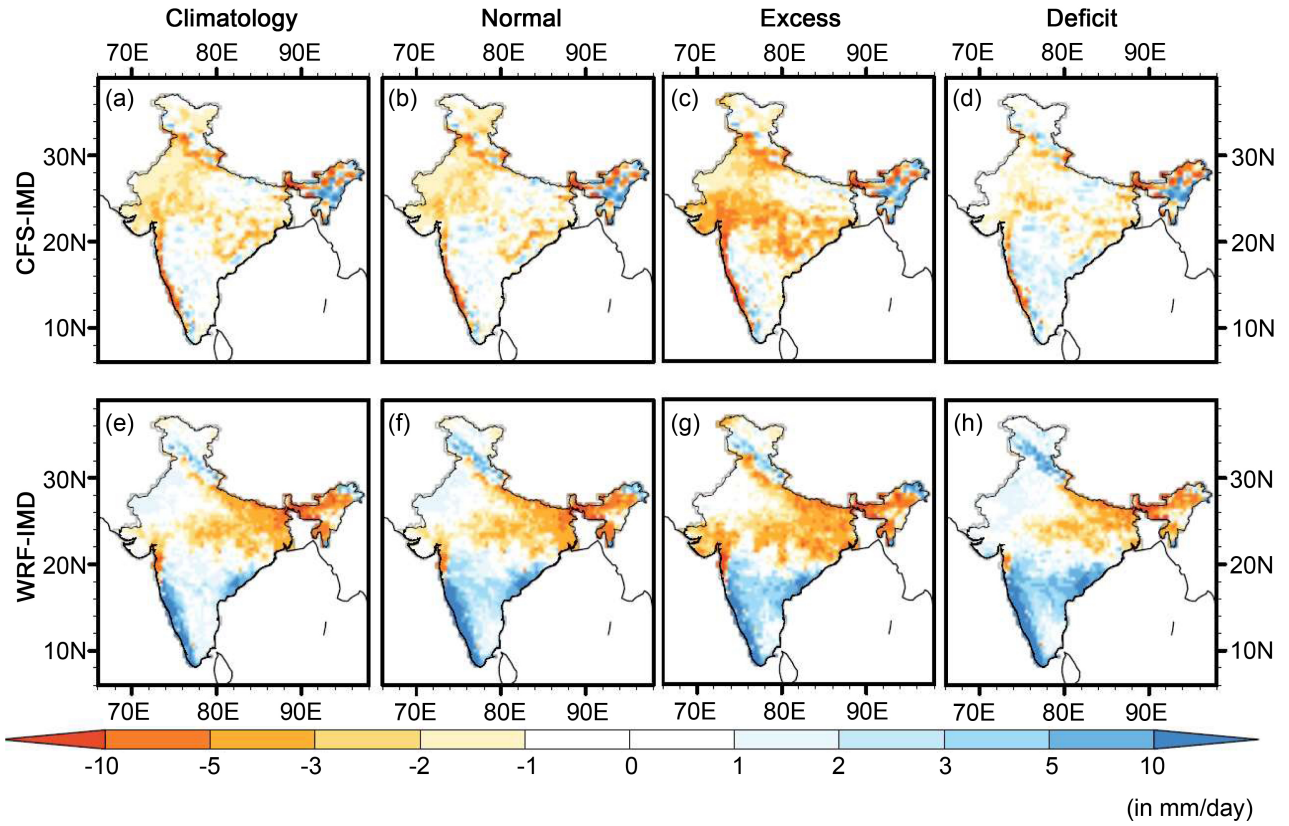

Figure 2. Mean rainfall bias (in mm/day) averaged (a) over the hindcast period of 1982-2008 and that of the composite (b) normal (c) excess and (d) deficit monsoon seasons as observed in IMD. Panels (e)-(h) and (i)-(l) are same as (a)-(d) but as simulated by CFSv2 and WRF respectively.

CFSv2 possess a dry bias over most of India whereas the WRF has a dry bias over the Gangetic plains for the excess monsoon season. Most of the regions are associated with wet bias with the WRF model. Over the Western Ghats, the wet bias is quite higher with the WRF model. The bias is around 2 - 10 mm/day over the Western Ghats. On a climatological scale, the WRF has better performance compared to the CFSv2 where the biases are reduced significantly with the downscaling experiments. During the excess monsoon season, the WRF possess dry bias over the Gangetic plains by 2 - 5 mm/day. This may be arising due to the excessive rainfall over eastern India such as Odisha and Andhra Pradesh where there is excessive rainfall, meaning most of the moisture transported from the ocean surface is recycled over these regions rather than getting advected towards the central India. The biases in CFSv2 are quite similar which signifies that the CFSv2 possess certain systematic biases and tends to simulate the model climatology rather than capturing the seasonality of the monsoon.

Figure 3 shows the monthly rainfall climatology of the four months involved with the summer monsoon as observed in the IMD and as simulated by CFSv2 and WRF. The rainfall received over India is maximum for the month of August followed by July, September and June. A model can be considered to be skillful if the rainfall is simulated well in each of the monsoon months. Similar pattern of

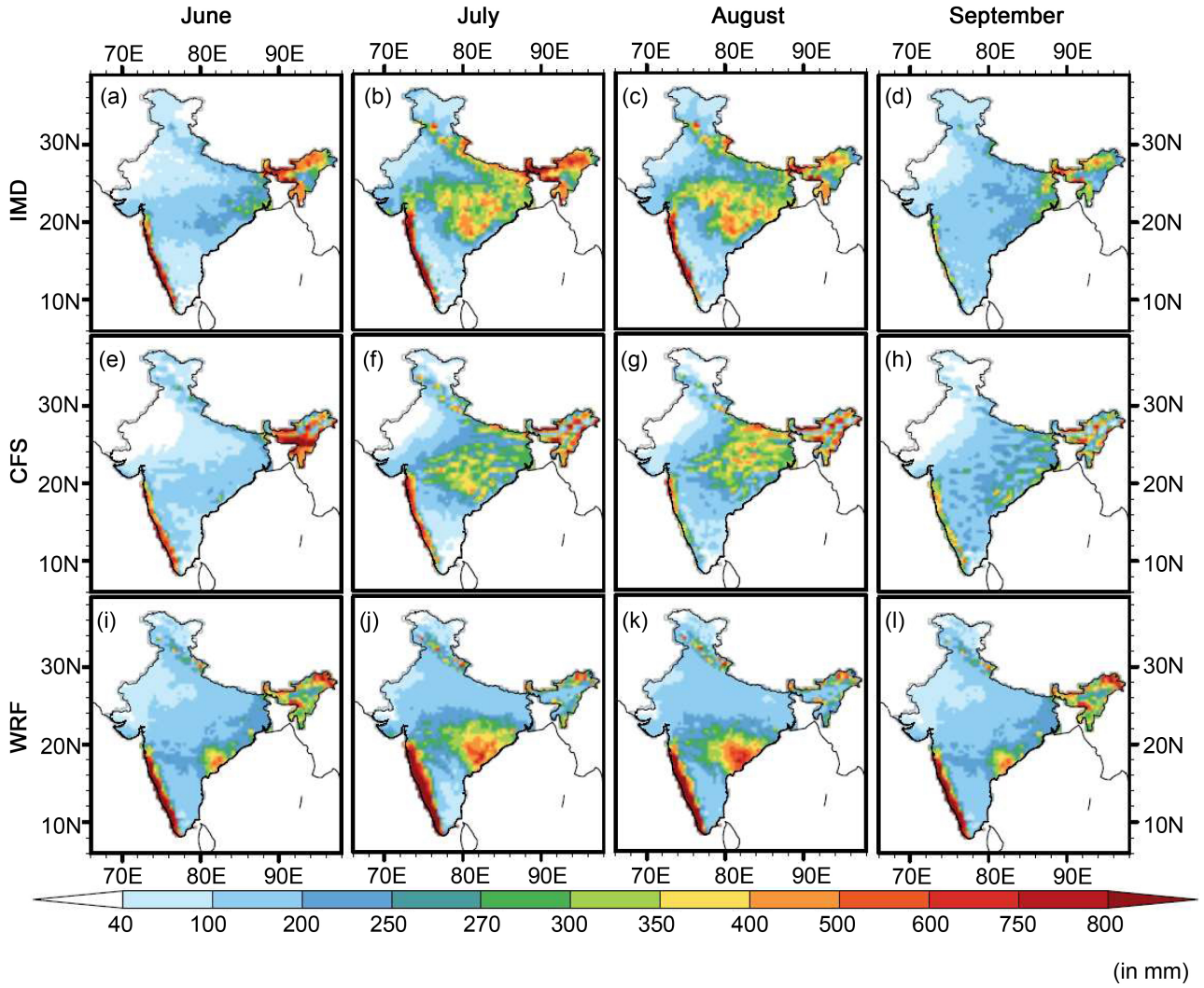

Figure 3. Monthly rainfall (in mm) climatology of the months June, July, August and September over the period of study as observed in IMD and as simulated by CFSv2 and WRF respectively.

rainfall is observed with the CFSv2 as well as WRF. The WRF model tends to overestimate the rainfall over small regions of the east coast of India as well as the Western Ghats during the months June and September. The monthly rainfall is overestimated by 200 - 400 mm with the WRF model over some regions of the eastern coast of India. In the CFSv2 model, the rainfall is overestimated over the northeast India during the month of June. The rainfall over the Western Ghats is highly overestimated in all the months with the WRF model where the model simulates the rainfall above 800 mm during all the months of the monsoon season. **Figure 4** shows the probability density functions of the daily rainfall climatology of the IMD, CFSv2 and WRF simulated rainfall averaged over all the grid points combined and the right panel shows the Taylor's diagram showing the correlation coefficients, standard deviation, RMSE and the relative bias in the CFSv2 and WRF model simulated rainfall with respect to the IMD data set. The normal distribution curves are fitted based on the Gaussian fits for the rainfall

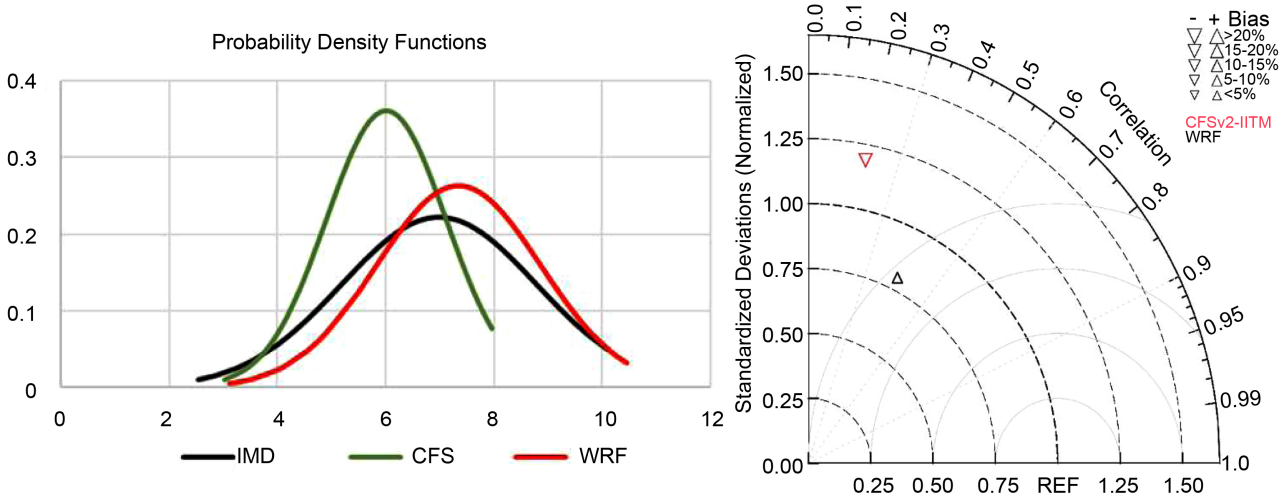

Figure 4. Probability density functions of the daily rainfall climatology of IMD, CFSv2 and WRF (Left panel). The rainfall is fitted to normal distribution to generate the Gaussian curves. Taylor diagram showing the correlation coefficients, standard deviation, RMSE and relative bias of the seasonal rainfall climatology with the CFSv2 and WRF simulated rainfall with respect to IMD (Right panel).

over all the grid points over India. The normal distribution of rainfall in the IMD dataset shows that the rainfall is distributed over a long range of 2.5 - 10 mm/day during the monsoon season. The distribution of rainfall is quite heterogeneous due to the inhomogeneity of the spatial rainfall distribution and the intra seasonal variability of the monsoon rainfall. The CFSv2 simulated rainfall has a very short range of distribution as compared to the IMD rainfall. The rainfall with CFSv2 is distributed within the range of 3 - 8 mm/day with maximum concentration at 6 mm/day levels. The model tends to simulate the climatological rainfall which can be inferred from Figure 1 and Figure 3. The WRF rainfall is quite similarly distributed to the IMD rainfall having the range of distribution spread over 3 - 10.5 mm/day. Maximum probability of rainfall is observed at 6.5 mm/day in the IMD data set which is 6 mm/day in the CFSv2 and 7 mm/day in the WRF model.

The Taylor diagram represents the rainfall statistics computed for the seasonal rainfall over the entire period of study with respect to the IMD rainfall. The pattern correlation coefficients, error statistics are computed for the mean seasonal rainfall over the 28 years of study. The skill of the WRF model in simulating the seasonal rainfall improves significantly as compared to the parent GCM, CFSv2. The temporal correlation coefficient is improved from 0.21 with CFSv2 to 0.38 with the WRF model. The RMSE is reduced from 1.2 with the CFSv2 to 0.81 with the WRF model. The relative bias is more than −10% in the CFSv2 model whereas the relative bias is within 5% - 10% in the WRF model. The WRF model thus helps in improving the forecasts from CFSv2 which can be inferred from the skill scores. The dynamic downscaling process can help in improving the rainfall forecasts skill. Table 2 shows the correlation coefficients, mean seasonal rainfall, MPE and PSE for the WRF and CFSv2 simulated rainfall over India and

Table 2. Climatological mean (mm), correlation coefficients (CCs), mean percentage error (MPE), phase coherency (PSE) and standardized anomaly index error (SAIE) between IMD rainfall, CFS and WRF simulated rainfall over all India (AI) and its homogeneous region during JJAS 1982-2008.

		HRI	NWI	CNEI	NEI	WCI	PI	AI
Mean (mm)	IMD	708	520	933	1422	956	723	875
	CFS	688	398	1071	1601	823	607	701
	WRF	899	439	820	1324	997	1072	928
CCs	CFS	0.43	0.11	0.17	0.19	0.21	0.19	0.21
	WRF	0.53	0.31	0.44	0.31	0.48	0.21	0.38
MPE (%)	CFS	−2.73	−10.50	14.09	12.59	27.04	66.93	17.13
	WRF	−4.49	−15.56	−11.36	14.16	20.28	48.25	12.78
PSE (%)	CFS	48	52	70	56	52	37	48
	WRF	70	70	78	63	56	44	78

the rainfall homogenous regions of India. From the mean rainfall it can be inferred that the CFSv2 underestimates the rainfall whereas the WRF overestimates it. Over the homogenous regions of India, the CFSv2 possesses large dry bias over the northwestern India, hilly regions of India and the peninsular India. The WRF corrects the deficient rainfall over northwestern, central northeast India. But the WRF simulates excessive rainfall over the hilly regions the peninsular India. The climatological all India rainfall as observed at 875 mm which is underestimated at 701 mm with CFSv2 and overestimated with the WRF at 928 mm. The correlation coefficients are improved significantly with WRF over India, central India, northwestern and hilly regions of India. The mean percentage error in the climatological rainfall is reduced with the WRF model as well. The all-India rainfall errors are reduced from 17% to 12% by the method of downscaling. Similarly, the phase synchronizing events are more simulated in the WRF as compared to the CFSv2 rainfall. This means that the WRF model helps in capturing the rainfall anomalies for a particular season. The PSE for all India rainfall is improved from 48% with CFSv2 to 78% with WRF. This signifies that a greater number of seasons indicates the extremity of a particular season with the dynamically downscaled rainfall. Table 3 shows the correlation coefficients and the mean rainfall bias over the homogenous rainfall regions but separately for the excess, normal and deficit years. Most of the regions show improvement in reducing the bias with the WRF model for the composite years. The correlation coefficients are improved from the CFSv2 and are significantly improved in the extreme years.

Figure 5 shows the time series of the mean seasonal rainfall and the standardized anomaly index of the rainfall observed in the IMD dataset and as simulated by CFSv2 as well as WRF models over the hindcast period of 1982-2008. From the time series, the intra-annual variability can be clearly identified in the

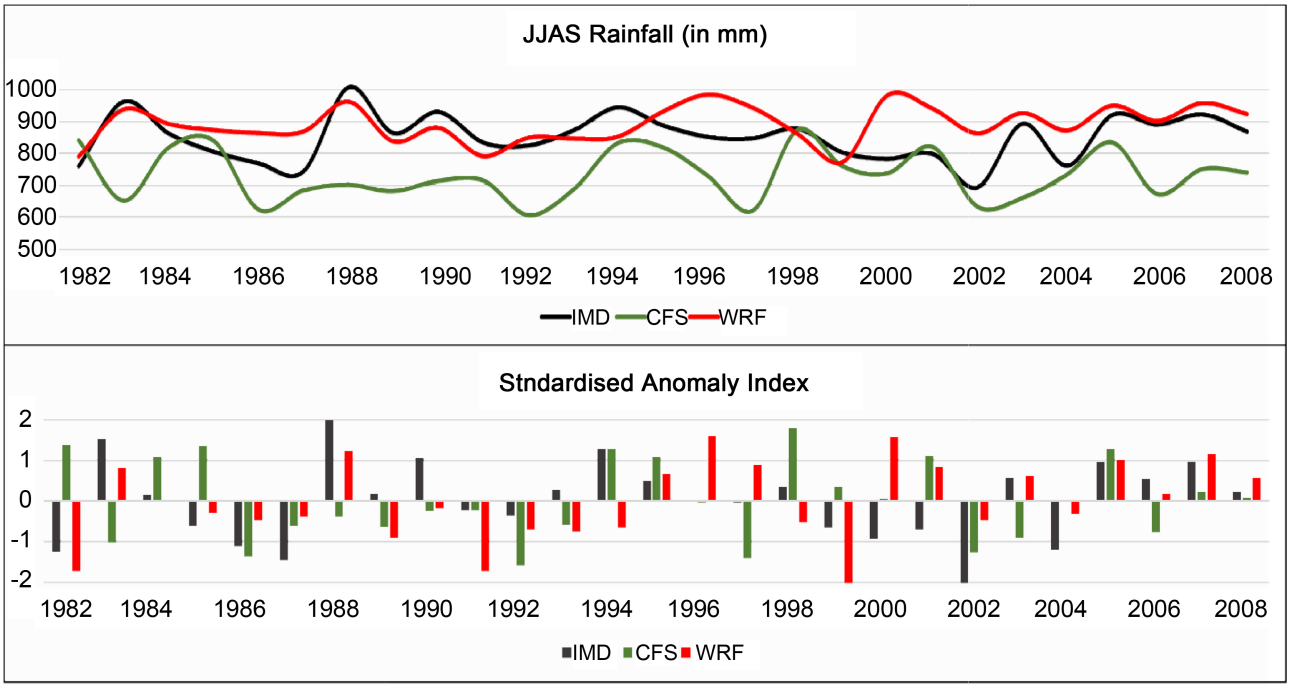

Figure 5. Time series of the mean seasonal rainfall (in mm), averaged all over India as observed in IMD, and as simulated by CFSv2 and WRF over the entire period of study (Top panel). The bottom panel is the same as the top panel but for Standardized rainfall anomaly index.

IMD data set where the rainfall ranges between 700 - 1000 mm. Some particular seasons have excess rainfall whereas some of the seasons produce scanty rainfall. Anomalous rainfall can be witnessed in some extreme years such as 1982, 1987, 1988, 1994, 2002, etc. The CFSv2 underestimates the rainfall for most of the seasons whereas the WRF model produces the rainfall closer to the observations for more years as compared to CFSv2. The standardized anomaly index of seasonal rainfall shows that the rainfall anomaly is in agreement with most of the years over CFSv2. The CFSv2 rainfall anomaly is in the same phase to that of IMD anomaly index for 13 years out 27 whereas the WRF is in the same phase for 19 out of the 27 years used in this study. This is also supported by the PSE skill score for the rainfall homogenous regions as well as all India rainfall (Table 2).

3.2. Upper Air Parameters

The rainfall, although being the most important meteorological parameter of highest societal interest, is quite a complex process and is highly influenced by the large scale as well as the small-scale parameters. In order to understand the impact of some of the significant physical parameters influencing the rainfall, some of the upper air and surface parameters have been analyzed in this section.

The mean seasonal winds at 850 hPa as observed from the ERA5 and as simulated by CFSv2 and WRF averaged over all the years used in this study and over the composites of excess, normal and deficit monsoon seasons are shown in Figure 6. The low-level jet stream over the Arabian sea is one of the most important features of the summer monsoon that influences the onset, intensity and

Table 3. Correlation coefficients and the mean seasonal rainfall bias (mm/season) for the JJAS precipitation between the observed IMD rainfall data set and CFS as well as WRF simulated rainfall over India and six homogeneous regions for the composite deficit, excess and normal summer monsoon seasons between the years 1982-2008.

	Composite deficit India summer monsoon season			
	CCs		Rainfall Bias (mm/JJAS)	
	CFS	WRF	CFS	WRF
AI	0.37	0.42	−163	62
HRI	0.32	0.51	−212	125
NWI	0.02	0.36	−196	76
CNEI	0.28	0.53	−96	189
NEI	0.41	0.59	174	−296
WCI	0.17	0.21	−121	−108
PI	0.39	0.21	−187	266
	Excess			
	CCs		Rainfall Bias (mm/JJAS)	
	CFS	WRF	CFS	WRF
AI	0.13	0.48	−344	122
HRI	0.36	0.53	−232	224
NWI	0.12	0.28	−321	102
CNEI	0.21	0.39	−210	−78
NEI	0.07	0.11	−407	−129
WCI	0.18	0.29	−215	−56
PI	0.20	0.34	−112	245
	Normal			
	CCs		Rainfall Bias (mm/JJAS)	
	CFS	WRF	CFS	WRF
AI	0.16	0.46	−173	43
HRI	0.55	0.55	−97	107
NWI	0.19	0.37	−203	15
CNEI	0.09	0.37	−178	125
NEI	0.05	0.15	124	−76
WCI	0.27	0.68	−285	164
PI	0.13	0.60	−325	104

advancement of the monsoon into the Indian main land region. In the ERA5 reanalysis data set, it can be seen that the intensity of the low-level jet stream reaches about 20 - 25 m/s which varies by 2 - 5 m/s in the excess and deficit monsoon seasons. Much variability is not observed in the contrasting monsoon seasons. Thel ow-level jet brings moisture laden winds from the ocean surface

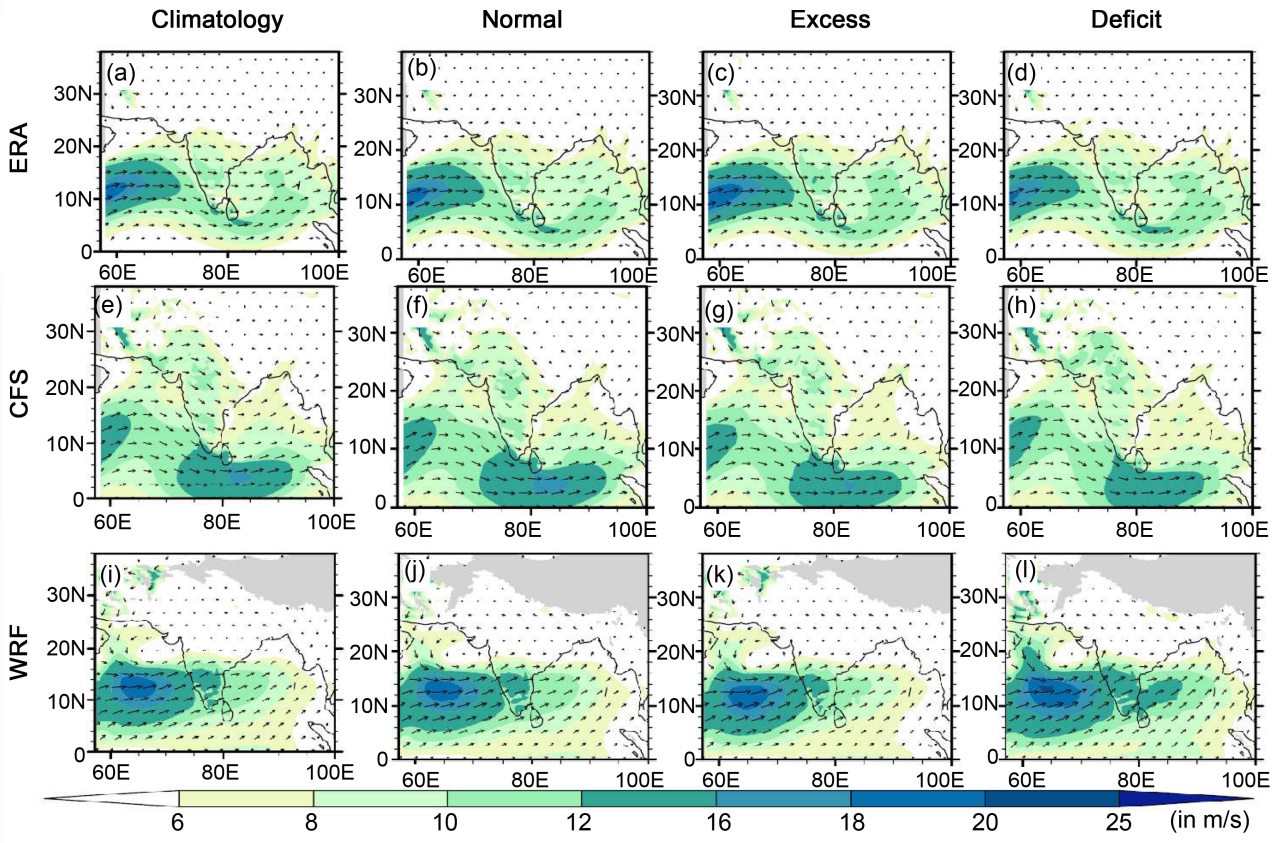

Figure 6. Mean seasonal (JJAS) wind (in m/s) and wind direction at 850 hpa averaged (a) over the hindcast period of 1982-2008 and that of the composite (b) normal (c) excess and (d) deficit monsoon seasons as observed in ERA dataset. Panels (e)-(h) and (i)-(l) are same as (a)-(d) but as simulated by CFSv2 and WRF respectively.

into the land region which is one of the primary contributors to the monsoon rainfall. Accurate simulation of the 850 hPa winds over the Indian monsoon domain is essential for a dynamical model to capture the rainfall pattern and intensity over the land region. The CFSv2 fails to simulate the pattern and intensity of the low-level jet streams. The regions maximum wind is observed over the Arabian sea but the intensity ranges between 10 - 20 m/s as compared to 20 - 25 m/s in the observed data set. This may a reason for the inadequacy of the CFSv2 in simulating the rainfall over India, particularly over the Western Ghats. The winds over some regions of the Bay of Bengal are overestimated in the CFSv2 model. The WRF model captures the 850 hPa winds better than the CFSv2. Though the regions with maximum winds are shifted eastwards, the intensity is quite closer to the ERA5 data set. This peculiar property of eastwards shifting of the high winds region might be arising due to the positioning of the lateral boundaries in the WRF model. The WRF model is initialized with the CFSv2 output and the weaker winds in the CFSv2 might be hampering the simulation of winds in the WRF model. Over the peninsular India, the WRF model overestimates the winds which may be a reason for the enhanced precipitation over this particular region. The biases over the Bay of Bengal in the CFSv2 is reduced in the WRF model which reproduces quite closer pattern of winds to that of the

ERA5 dataset. However, there is an anomalous cyclonic circulation over the north Arabian Sea in the WRF model. This anomalous circulation if found for all the composite years and may be arising due the systematic bias in the WRF model.

The tropical easterly jet stream at 200 hPa levels is also another typical feature of the Indian summer monsoon which drives the large scale circulation and is an important component of the monsoon Hadley cell. Figure 7 shows the winds at 200 hPa in a similar fashion to that of the 850 hPa winds. The tropical easterly jet streams are quite well captured by both the CFSv2 and WRF models. The anti-cyclonic circulation over the Tibetan plateau drives the overturning to the mid-latitude circulation which further transforms into the Hadley cell. This particular overturning of the winds at 200 hPa is quite well simulated in both the models. The WRF model reproduces the wind pattern closer to the ERA5 as compared to the CFSv2. The wind intensities are quite similar in all the composite years as well as the climatological value. Maximum winds are observed over the Tibetan plateau which reduces gradually southwards and increases over the

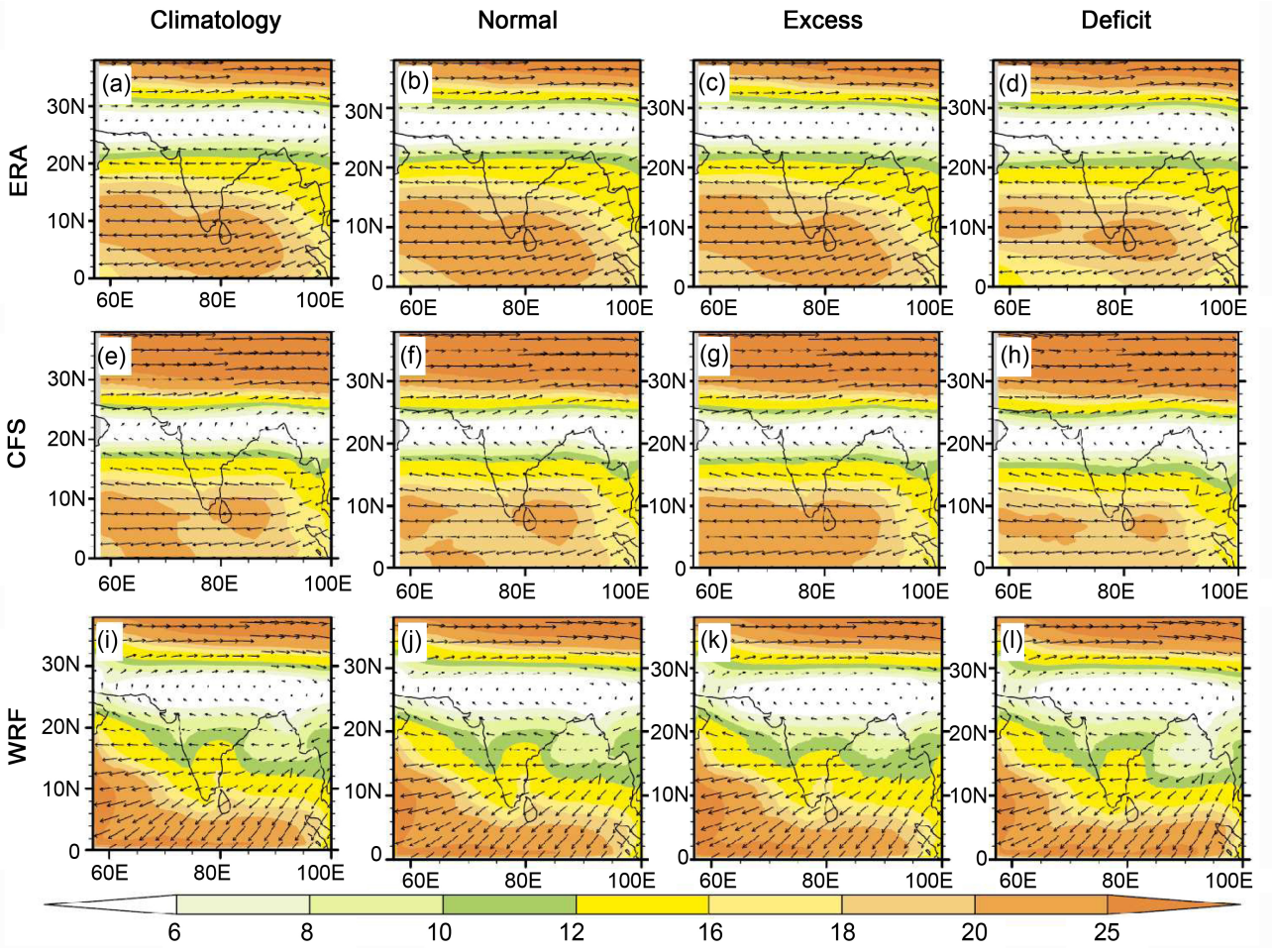

Figure 7. Mean seasonal (JJAS) wind (in m/s) and wind direction at 200 hpa averaged (a) over the hindcast period of 1982-2008 and that of the composite (b) normal (c) excess and (d) deficit monsoon seasons as observed in ERA dataset. Panels (e)-(h) and (i)-(l) are same as (a)-(d) but as simulated by CFSv2 and WRF respectively.

Indian ocean region. Over the Indian ocean, the winds range between 12 - 25 m/s in the ERA5 dataset which is at 10 - 18 m/s and 12 - 30 m/s in the CFSv2 and WRF model respectively. Minimum wind regions lie between the Himalayas and the Gangetic plains. The regions of minimum winds are observed over the ERA5 as well as all the model simulations.

Figure 8 shows the mean 2-meter temperature and the mean sea level isobars averaged over the entire period of 27 years during the monsoon season. The surface temperature is an important parameter that influences the simulation of moisture and thermodynamics of the model and ultimately rainfall. From the spatial pattern of temperature, it can be seen that the temperatures are maximum over the northwestern India and are lesser over the Western Ghats and adjoining areas. The CFSv2 model has a significant warm bias over the northern India and especially over the Gangetic plains. The warm bias is reduced in the WRF model, and the temperature pattern is closer to the ERA5 with the WRF model as compared to the CFSv2 model. However, the warmer temperatures over the eastern coast of the southern peninsula region (coastal regions of southern Andhra Pradesh and Tamilnadu) are not simulated by the WRF model. This may be arising because of the wet bias over these regions in the WRF model. Wet bias over these regions may be leading to the cooling of the surface temperatures and lesser precipitation recycling ratio. The mean sea level isobars in the ERA5 show that the high-pressure regions are over the Tibetan plateau and over the equatorial region. The isobars closely follow the temperature contours which suggests that the temperatures play an important role in the simulation of the mean sea level pressures. Higher pressures of 1010 - 1020 hPa are seen over the Tibetan plateau. The isobars are similarly simulated with the CFSv2 as well as the WRF model. But the high pressure over the Tibetan plateau is underestimated with the CFSv2 model which is corrected by downscaling with the WRF model. Over the Tibetan plateau, the pressure simulated by CFSv2 is 1010 - 1015 hPa and is 1010 - 1020 hPa with the WRF model. Over the equatorial Indian

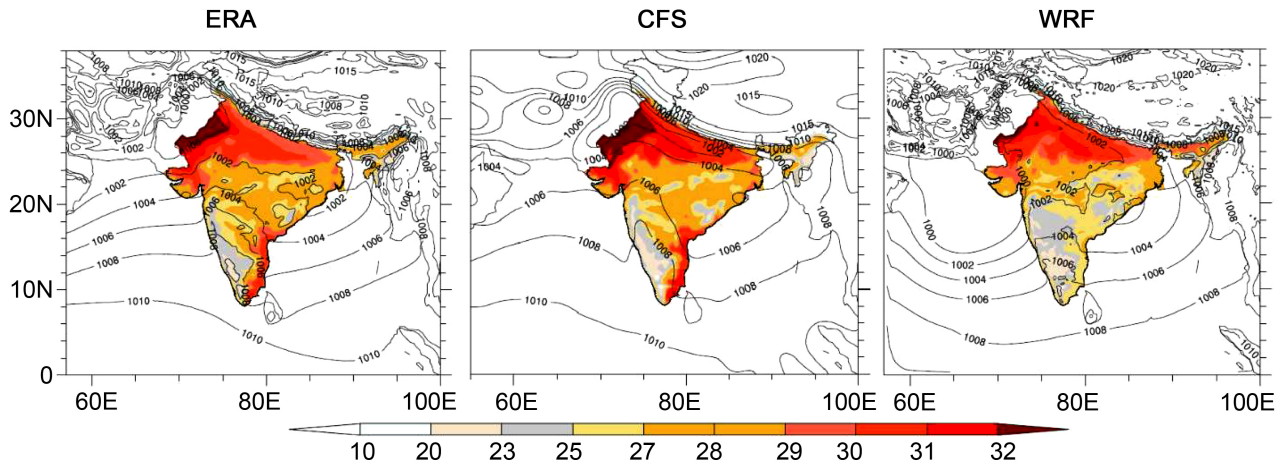

Figure 8. Mean seasonal (JJAS) 2-meter temperature (shaded contours) and mean sea level pressure isobars (contour lines) averaged over the hindcast period of 1982-2008 as (a) observed and as simulated by (b) CFSv2 and (c) WRF.

ocean, the CFSv2 simulates the mean sea level pressure closer to the ERA5 data set as compared to the WRF model. Analogous to the anomalous lower-level cyclonic circulation in the WRF model, the sea level pressure is lower than normal in the northern Arabian Sea. The lower MSLP might be creating anomalous cyclonic circulation over these regions. This may be a persistent systematic bias in the WRF model while using the CFSv2 data as ICBC.

Relative humidity along the vertical column of the atmosphere controls the cloud parameters and the conversion of water vapor to rainfall in the atmosphere. Figure 9 shows the climatological seasonal relative humidity averaged

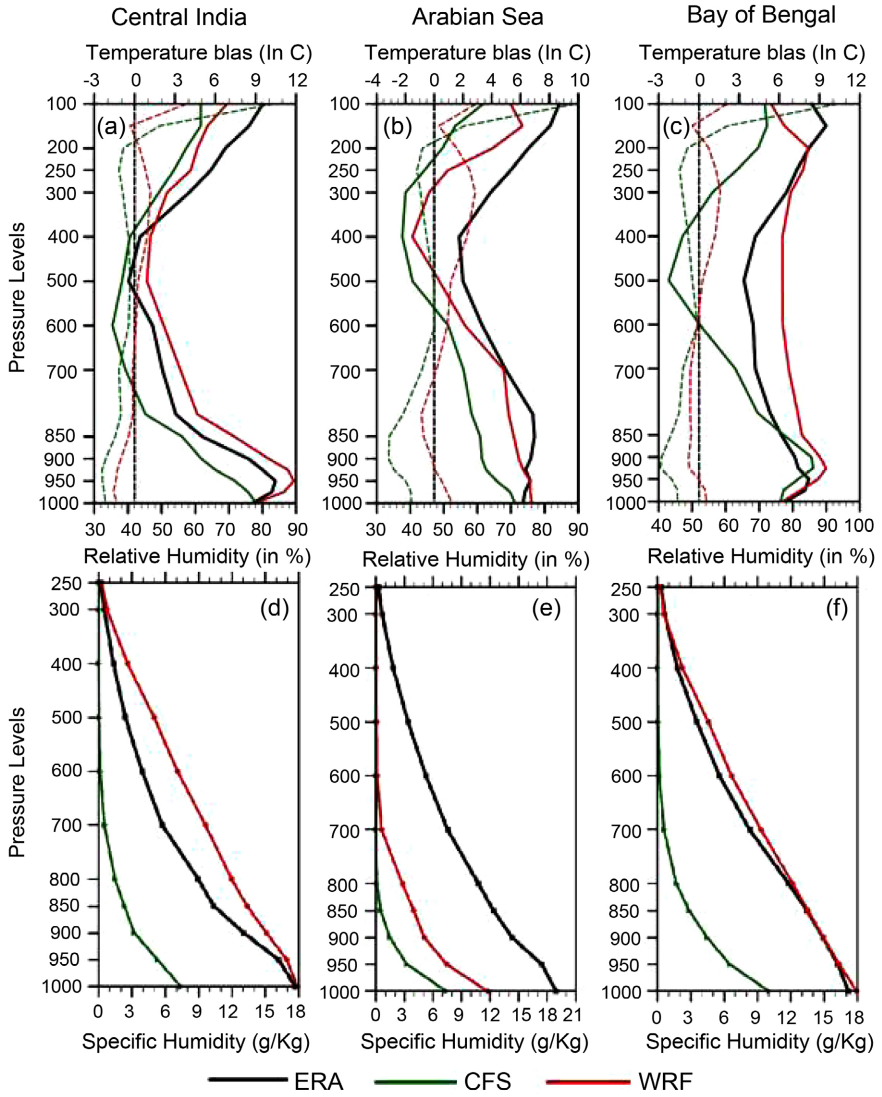

Figure 9. Vertical profile of the relative humidity (solid lines) and temperature bias (dashed lines) over the entire column of the atmosphere, averaged over the hindcast period of 1982-2008 as (a) observed and as simulated by (b) CFSv2 and (c) WRF. The areas over which the profiles are computed are (a) central India (90N - 240N, 720E - 840E), (b) Arabian sea (130N - 180N, 640E - 690E) and (c) Bay of Bengal (110N - 160N, 850E - 900E). The bottom panels are computed for the same areas of (a), (b) and (c) but for specific humidity along the entire column of the atmosphere.

over the vertical column of the atmosphere from the surface to 100 hPa pressure level. The relative humidity is maximum over the Bay of Bengal as compared to the Arabian sea (**Figure 9(d)**) in the observed ERA5 dataset. Over the oceans, the moisture availability is maximum as compared to that over the land surface but the differences in the spatial pattern over the oceans can be attributed to the eastward advection of the moisture due to the low-level jet stream over the Arabian sea. Maximum relative humidity can be observed over the Western Ghats where the mountainous regions act as a barrier to moisture and wind. Over the Indian main land region, the relative humidity is minimum over the arid regions of Thar desert and northern Himalayas. The relative humidity is not well captured by the CFSv2 model over the land as well as the oceans. The biases are much over the land region and especially over the wet land of the eastern India which is home to many river systems and ample amount of moisture is transported into the land surface from the Bay of Bengal. The WRF model overestimates the relative humidity over the Arabian sea as well as over Bay of Bengal. Over the land, it follows a closer pattern to that of observation.

The vertical profiles of the relative humidity and the temperature biases over central India, Arabian sea and Bay of Bengal are shown in **Figures 9(a)-(f)**. The vertical profile is computed over these three distinct regions as they have some peculiar characteristics, and the relative humidity pattern is different over these three regions. The regions of computation are central India (9˚N - 24˚N, 72˚E - 84˚E), Arabian sea (13˚N - 18˚N, 64˚E - 69˚E) and Bay of Bengal (11˚N - 16˚N, 85˚E - 90˚E). The relative humidity from the ERA5 reanalysis data shows that the relative humidity increases up to a few kilometers above the surface after which it decreases till 500 hPa levels after which the relative humidity starts increasing again till the top of the atmosphere (**Figure 9** solid black lines). Over the central India region, the relative humidity profile of the CFSv2 and WRF are quite closer to ERA5. But over the oceanic regions, the relative humidity profile varies quite largely. The CFSv2 has weaker relative humidity representation at 700 - 200 hPa levels which is corrected with the WRF model. Over the Bay of Bengal, the simulation of relative humidity is weaker than the Arabian sea. The WRF performs better in representing the relative humidity profile than the CFSv2. The relative humidity comes to a minimum value at 500 hPa over the land as well as ocean regions. At 500 hPa, the relative humidity is 40%/35%/60% with the ERA/CFSv2/WRF over the central India region. The same is 65%/40%/45% and 70%/45%/75% over Arabian sea and Bay of Bengal respectively. The temperature biases of the CFSv2 and WRF with respect to ERA5 along the vertical column of the atmosphere is shown in **Figures 9(a)-(c)** with dashed lines. The CFSv2 shows a cold bias over most of the vertical pressure levels (1000 - 200 hPa) whereas the WRF shows cold bias from the surface to 500 hPa levels after which the WRF shows a warm bias up to the top of the atmosphere. However, the cold biases are reduced with the WRF as compared to CFSv2. The CFS shows a cold bias of −2.5/−3/−3˚C over central India/Arabian

sea/Bay of Bengal (Figure 9 dashed green lines) as compared to −1.5/0.5/0.5˚C over central India/Arabian sea/Bay of Bengal with the WRF (Figure 9 dashed red lines) respectively.

The specific humidity profiles over the same regions as that of relative humidity are shown in Figures 9(a)-(c). The specific humidity along the vertical quantifies the net precipitable water and hence can give an idea about the rainfall over a particular region. The specific humidity is not quite well simulated in the CFSv2 model which underestimates the specific humidity over the monsoon core zone as well as the oceans. The WRF has similar pattern and intensities to that of the ERA5 specific humidity over the land region and Arabian Sea. Over the central India region and Bay of Bengal, the WRF overestimates the specific humidity between 800 - 400 hPa which may be the reason for excessive rainfall over the eastern coast and peninsular India.

3.3. Diabatic Heating

The vertical residual heating distribution drives the monsoon circulation (Waliser 2006) and different modes of variability are also largely modulated by the vertical heating distribution (Goswami *et al.* 2013). The large-scale vertical heating source (Q1) over the central India (9˚N - 24˚N, 72˚E - 84˚E), Arabian sea (13˚N - 18˚N, 64˚E - 69˚E) and Bay of Bengal (11˚N - 16˚N, 85˚E - 90˚E) is shown in Figure 10. The vertical heat source and moisture sink are computed following Yanai *et al.* [62] and also as used by various other studies [63]. The ERA heating profile (Q1) shows (Figure 10, nold line) a lower-level maximum around 750 - 700 hPa and a middle level maximum at around 400 hPa, suggesting

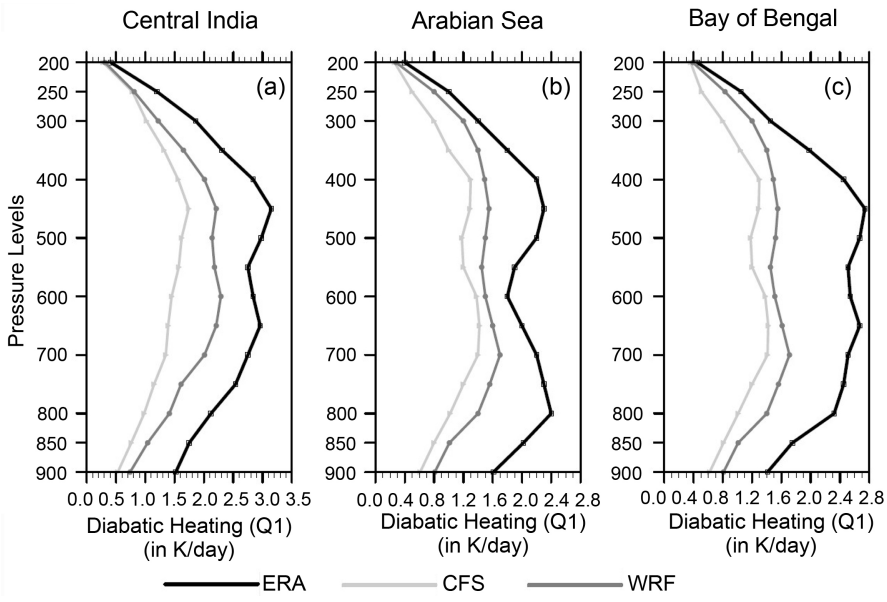

Figure 10. Diabatic heating (Q1) profile (time and domain averaged) from 900 hpa to 200 hpa pressure levels, averaged over the hindcast period of 1982-2008 as (a) observed and as simulated by (b) CFSv2 and (c) WRF. The areas over which the profiles are computed are same as that of Figure 9.

a dominant heat source due to condensation (lower level) and other microphysical transition in the middle troposphere. Similar pattern is observed over the land as well as the ocean regions. The vertical structure of the diabatic heating shows that the thermodynamics pertinent to both convective and stratiform convection processes greatly influence the Indian monsoon rainfall. In the CFSv2 model, the heating profile is underestimated. The lower-level heating over the land region is comparatively shallow in the CFSv2 model. However, in the WRF model, the heating profiles are comparatively better and closer to the observations.

The discrepant residual heating of the CFSv2 and WRF may affect the moisture sink and the heat sources in the atmosphere. This factor may affect the divergence of wind in the upper atmosphere and convergence in the lower level. An unrealistic local Hadley cell may arise due to this in the model which may subsequently affect the vertical transport of moisture and ultimately affect rainfall. The negative heating biases in the vertical might be a reason for dry bias and lesser rainfall in the models over the selected regions. The microphysical transitions control the heating profiles which in turn are dependent on the hydrometeor mixing ratios prescribed in the various microphysics schemes [64] [65]. The impacts of different convective closures on systematic biases of Indian monsoon precipitation climatology have been analyzed by looking at the heating profiles and residual heating in the atmosphere influence the simulation of convective as well as non-convective rainfall in a dynamical model (Mukhopadhyay *et al.* 2010). In another modelling study, Benedict *et al.* (2013) concluded that simulation of the spatial structures of moistening and diabatic heating can help in simulating the convective disturbances in a GCM. Ling *et al.* (2013), stated that the convection over tropics is quite sensitive to the latent heating profiles. Consistent with the above studies, it seems that the unrealistic heat source profiles simulated by the dynamical models may be possibly due to the uncertainties associated with the microphysical, convective, and/or boundary-layer parameterizations. The impacts of different convective closures on systematic biases of Indian monsoon precipitation climatology have been analyzed by looking at the heating profiles and residual heating in the atmosphere influence the simulation of convective as well as non-convective rainfall in a dynamical model [66]. In another modelling study, Benedict *et al.* [67] concluded that simulation of the spatial structures of moistening and diabatic heating can help in simulating the convective disturbances in a GCM. Ling *et al.* [68], stated that the convection over tropics are quite sensitive to the latent heating profiles. Consistent with the above studies, it seems that the unrealistic heat source profiles simulated by the dynamical models may be possibly due to the uncertainties associated with the microphysical, convective, and/or boundary-layer parameterizations.

3.4. Surface Heat Fluxes

Figure 11 shows the time averaged mean upward sensitive heat flux, latent heat

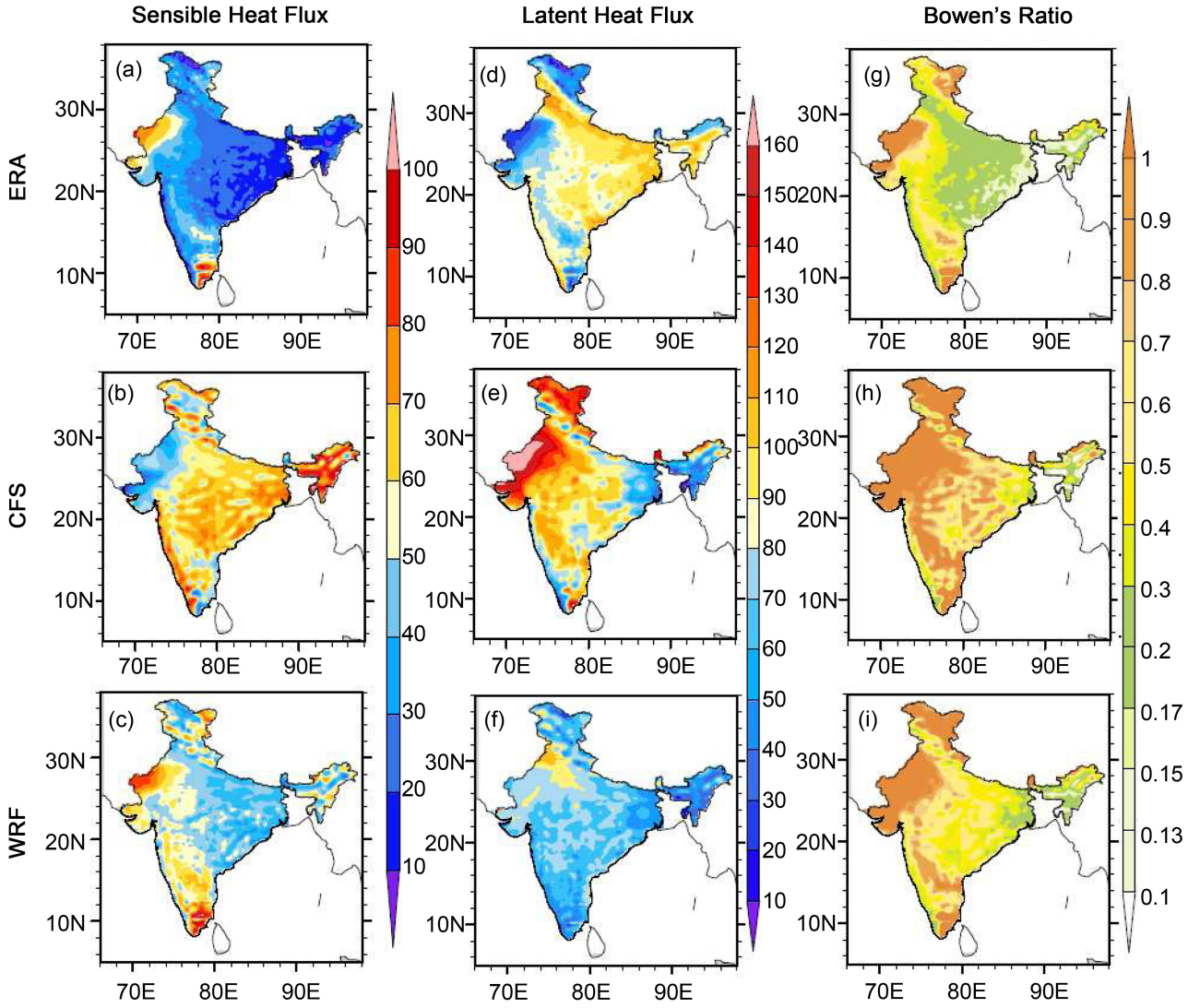

Figure 11. Upward Sensible heat flux (W/m^2), Latent heat flux (W/m^2) and Bowen's ratio over the Indian main land region as observed in ERA data set and as simulated by CFSv2 and WRF respectively. The fluxes are averaged over the entire hindcast period of 1982-2008.

flux and the Bowen's ratio during the JJAS period over the years 1982-2008. The surface heat fluxes are an important parameter that helps regulating the evaporation from soil as well as control the precipitation recycling ratio. The Bowen's ratio gives a rough idea of the dominant heat flux over a particular region and indirectly signifies the amount of rainfall with respect to the radiation received over a particular region. Previous studies have shown that the sensible heat flux reduces with the onset of the monsoon whereas the latent heat flux increases as the monsoon advances. This phenomenon can be attributed to the fact that as the rainfall increases along the season, the land surface cools as compared to the highly heated land surface during the pre-monsoon season. Increased rainfall also results in enhanced moisture availability and hence enhanced evaporation. This leads to the increase in latent heat flux during the monsoon season [69]

[70]. A Bowen ratio is the ratio of sensible to latent heat flux and influences the boundary layer dynamics affects surface buoyancy flux that drives affects surface buoyancy flux that drives (Stevens, 2007) and affects the rate at which convective boundary layer deepens. The humidity in the boundary layer is set by the Bowen ratio [71] and impacts the efficiency of moist convection heat cycle (the ratio between mechanical work and energy input at the surface; [72]) and the distribution of shallow convection cloud base mass flux [73]. Boundary layer characteristics can be influenced by Bowen ratio as the surface forced atmospheric conditions can have two distinctive environments during the monsoon and pre-monsoon season.

The sensible and latent heat fluxes are quite opposite in nature during the monsoon season which can be clearly identified in **Figure 11(a)** & **Figure 11(d)**. The sensible heat flux is very low over the entire India land region sparing the rainfall scanty regions such as the northwestern India and southern tip of India along the Tamilnadu coast. Similarly, the latent heat flux is higher over most of the regions of India except the regions with high sensible heat flux. The CFSv2 fails to capture the sensible heat fluxes as well as the latent heat fluxes over most of the regions of India. High latent heat flux and low sensible heat flux are observed over the northwestern India which is quite contradictory to the ERA5. Inability of the model to simulate the heat fluxes closer to the observation closely linked to the failure of the CFSv2 in reproducing the rainfall pattern as well as the intensities during the monsoon season. The sensible heat fluxes over the monsoon core region range between 10 - 30 W/m^2 in the ERA5 as compared to 50 - 80 W/m^2 and 30 - 60 W/m^2 in the CFSv2 and WRF respectively. The latent heat fluxes over the monsoon core region range between 70 - 120 W/m^2 in the ERA5 as compared to 70 - 140 W/m^2 and 40 - 90 W/m^2 in the CFSv2 and WRF respectively. Upward heat fluxes from the surface are an important parameter that drives the boundary layer dynamics and convection over the grid point associated. The WRF model performs better than the CFSv2 in representing the heat fluxes and has closer representation of the sensible heat flux. Though the WRF model simulates weaker sensible and latent heat fluxes, it performs better than the parent CFSv2 model. The inability of the model in simulating the heat fluxes can be supported from the spatial pattern of Bowen's ratio (**Figures 12(g)-(i)**). The Bowen's ratio is higher over the northwestern and southern tip of India owing to the higher sensible heat fluxes whereas is lower over the rainfall regions such as central and northeastern India owing to the higher rainfall regions leading to higher latent heat flux. The CFSv2 model fails to capture the Bowen's ratio with respect to the ERA5 and has values ranging between 0.7 - 1 over most of the regions of India. The Bowen's ratio ranges between 0.15 - 0.7 in the ERA5 whereas it ranges between 0.3 - 0.6 in the WRF model.

The planetary boundary layer (PBL) height and the convective available potential energy (CAPE) averaged over the entire period of 27 years for the JJAS months is shown in **Figure 12**. The PBL height is the layer where there is maximum instability leading to active convection during the monsoon season. The

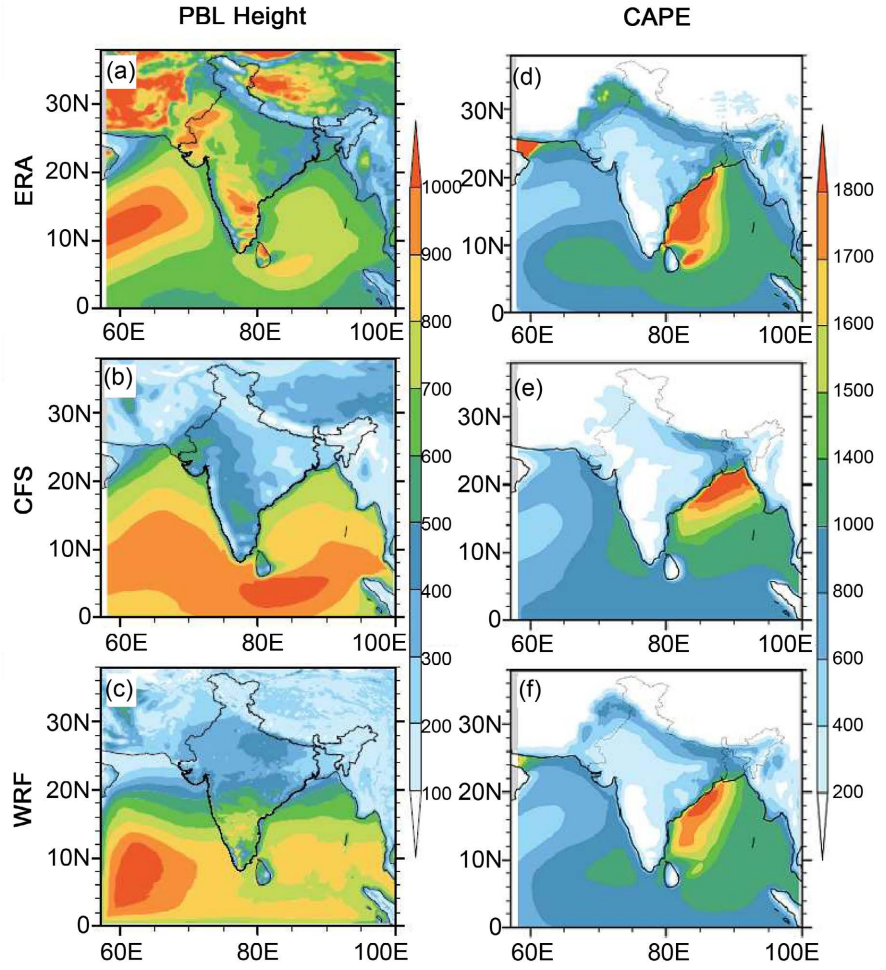

Figure 12. Mean boundary layer height as observed in (a) ERA and as simulated in (b) CFS and (c) WRF (Left column). The right column is same as left one (d), (e), (f) but for convective available potential energy integrated from the level of free convection to the equilibrium level.

PBL height in a dynamical model states the regions of maximum instability leading to active convection. The PBL height is also dependent on the upwards moisture convergence, surface temperature and other parameters. In the ERA5 dataset, the PBL height is maximum over the Arabian sea where there is maximum convergence of moisture and high transport of moisture by the low-level jet stream. The PBL height can vary in large numbers from a few tens of meters to a few kilometers. Though the PBL height is largely influenced by the diurnal cycle by the incoming solar radiation [74] [75] the variation on seasonal scale during the monsoon season can drive the changes in mean seasonal rainfall. Besides this, the growth and characteristics of PBL over land depends on multiple forcing mechanisms related to cloudiness, soil moisture, surface temperature, mesoscale convergence, low-level cold-air advection, and synoptic-scale subsidence [76] [77] [78].

The PBL is typically shallower over the oceans as compared over the land. But on a seasonal scale, the PBL is deeper over the oceans (**Figure 13(a)**). Deeper

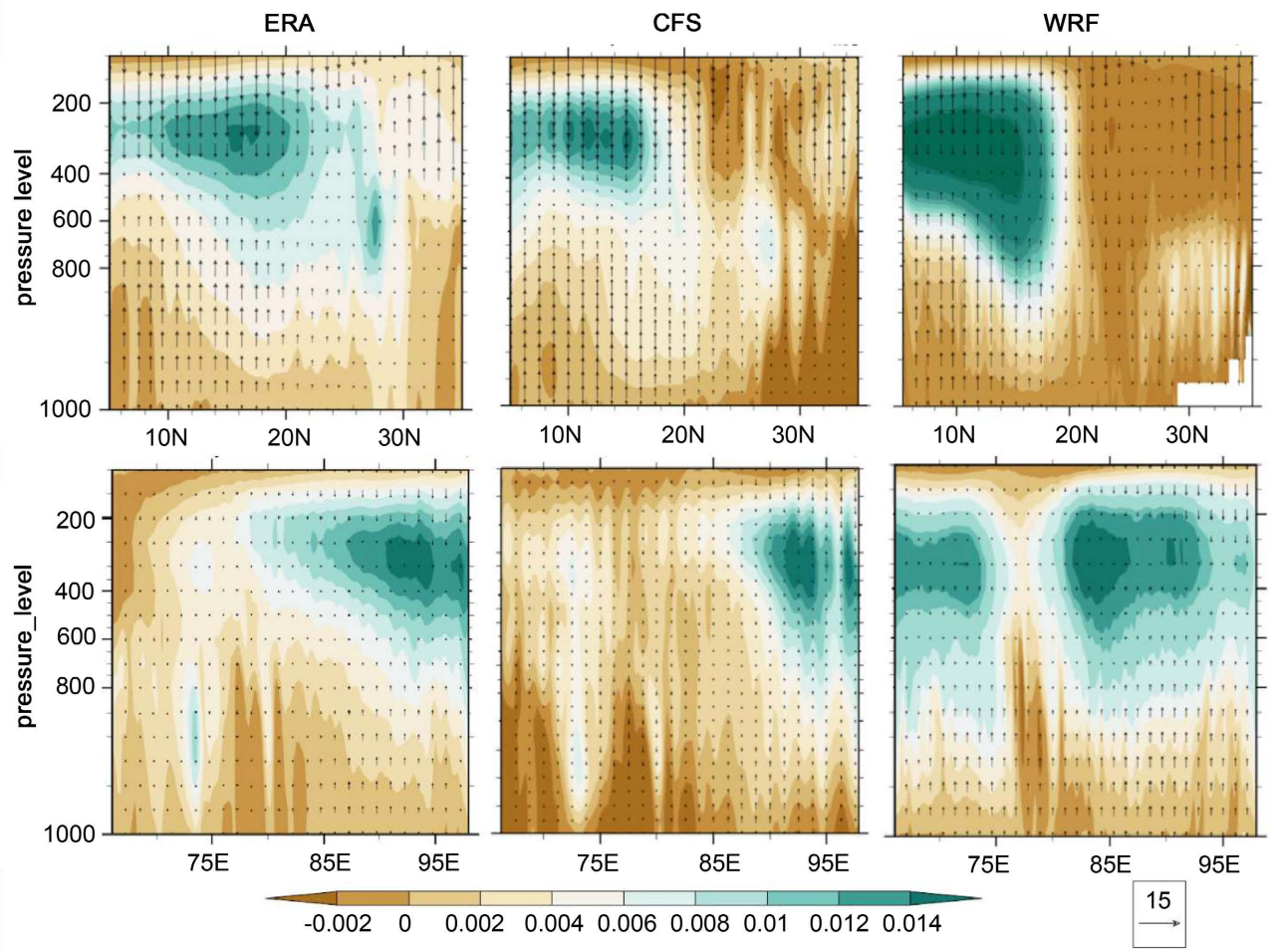

Figure 13. Vertical velocities averaged over the longitude (top panel) and latitude (bottom panel) over the entire period of simulation. The first column shows the ERA reanalysis vertical velocities whereas the second and third columns show the vertical velocities as simulated by the CFSv2 and WRF respectively.

PBL height is observed over the Arabian sea and rainfall scanty regions of India which ranges between 800 - 1000 m. The boundary layer is underestimated by the CFSv2 as well as WRF model. The WRF model has better representation of the PBL over the oceans as well as some parts of southern India. The rainfall pattern in the WRF is quite closer to the rainfall pattern simulated by the WRF model. The average PBL height is about 100 - 400 m in the CFSv2 as compared to 200 - 800 m in the WRF over the Indian main land region.

The CAPE is also an extremely important factor that contributes to the convective rainfall in a dynamical model. The CAPE is calculated as per the mathematical equation described in Section 2. The CAPE is higher over the Bay of Bengal as compared to the Arabian sea as well as the Indian main land region. Lesser CAPE over Arabian sea is quite similar to the pattern observed with the relative humidity which may be arising due to the advection of moisture due to the low-level jet stream. The CAPE over the Indian main land region ranges between 200 - 800 J/kg in the ERA5 data set as compared to 100 - 400 J/kg in the CFSv2 and 100 - 600 J/kg in the WRF model respectively. The CAPE is highly

underestimated with the CFSv2 as well as WRF model over the Gangetic plains and central India region which might be the reason for lesser rainfall over these regions.

The vertical velocities averaged over the longitude and latitude over the entire domain are shown in Figure 13. The vertical velocities determine the intensity of convection as well as orographic lifting which have a direct impact on the mesoscale convective activities. The errors in rainfall simulation arising in the dynamical models can be inferred from the pattern of vertical velocity in the models. Maximum updrafts are observed in the lower troposphere whereas the downdrafts are observed at upper troposphere at 200 - 400 hPa. Also, maximum upward and downwards motion of wind can be seen at the 10N - 20N and 85E - 95E. this may be arising due to the strong orographic lifting near the Western Ghats region and over the hilly regions of the northeast India. Though the vertical wind quantities are extremely small (0.01 - 0.02 m/s) as compared to the meridional or zonal wind, they do have an impact on the updrafts and downdrafts in the clouds which are responsible for strong convection.

The CFSv2 shows very low vertical velocities over central India region whereas the WRF shows high vertical velocities over the southern peninsula region. This can be attributed to the scanty rainfall over central India in CFSv2 model and heavy rainfall patches over Western Ghats in the WRF model. Similar observations can be found over the eastern part of the domain where the CFSv2 model shows excess downdrafts over the eastern part of the domain, over the hilly regions of northeast India and Myanmar. In the WRF model, biased downdrafts are observed in the western part of the domain at upper part of the atmosphere. Both the models show large biases in the rainfall sensitive regions of the domain which may be adding to the rainfall errors in the dynamical models.

4. Summary and Conclusions

This study is aimed at using the method of dynamical downscaling for the purpose of improving the skill of Indian summer monsoon rainfall forecast. The hindcast output from CFSv2 has been used to downscale using a high resolution WRF modeling system. The model has been simulated for a long period of 27 consecutive monsoon seasons to assess the skill of the model. The downscaled hindcast is compared with the observations as well as the parent GCM to assess the skill of the model in minimizing the errors and reproducing the meteorological parameters. A brief summary of the findings from this chapter can be discussed as:

The method of dynamically downscaling the CFSv2 hindcast using WRF performs quite well in improving the rainfall pattern as well as the intensities over the parent CFSv2. The seasonality of the monsoon along with the heavy rainfall patches over the Indian main land region is represented quite well with the WRF model. Significant areas of heavy rainfall patches such as the central India and Western Ghats are captured with the WRF which is completely missed in the

CFSv2 model. Composite analysis of the categorical monsoon seasons shows that the WRF outperforms the CFSv2 and produces the rainfall quite closer to the observations. Dry bias over most of India in CFSv2 is reduced with the WRF model especially for the composite deficit and normal monsoon seasons. The skill of the model is fairly improved from 0.21 to 0.38 with the CFSv2 and WRF respectively. Along with the skill, the rainfall distribution as well as mean seasonal rainfall errors are reduced with the WRF model.

The improvement in the rainfall can be attributed to the improvement in the representation of upper air and surface meteorological parameters. With the finer representation of the land surface at higher resolution, the surface fluxes and the moisture feedback between the land and atmosphere is improved in the WRF model. The parameters that have a direct impact on the rainfall are well simulated in the WRF model as compared to the CFSv2. Vertical structure of the relative humidity and heating profiles over rainfall significant regions over India show that the WRF model does a fairly good job compared to the CFSv2 in representing the vertical atmosphere. The surface heat fluxes are an important part of a dynamical model as they control the precipitation recycling ratio. The sensible and latent heat fluxes are represented quite closer to the observations in the WRF model which may be a reason for the better representation of the temperature and moisture gradients along the vertical column of the atmosphere in the WRF model. The semi-permanent features of the summer monsoon such as the low-level jet, tropical easterly jet, Tibetan high, etc., are represented better in the WRF model as compared to the CFSv2 model. The winds at 850 hPa are represented much better in the WRF model than the CFSv2 model and the wind structure for the extreme monsoon seasons varies significantly. The low-level jet streams are an important component of the monsoon Hadley cell which may be helping the WRF model in simulating the rainfall closer to the observational data sets of IMD. The precipitation pattern in the WRF model closely follows the PBL height and CAPE pattern. The cumulus convention in the WRF model is a function of the relative humidity which closely follows the lower-level turbulence and static stability. Since these parameters are fairly closer to the reanalysis data in the WRF model, they help in simulating the rainfall closer to the observations. Overall, the WRF fairly does a good job in simulating the Indian summer monsoon and rigorous methods such as ensemble downscaling methods, statistical methods for bias correction can be implemented to improve the skill of the WRF model further.

Acknowledgements

The authors acknowledge the IMD and ECMWF for providing observation and reanalysis datasets for the verification of the performance of the model. The first author acknowledges the University Grants Commission for providing the funding for carrying out research work. The authors are grateful to the IITM, Pune for providing the CFSv2 hindcast data.

Conflicts of Interest

The authors declare no conflicts of interest regarding the publication of this paper.

References

[1] Parthasarathy, B., Munot, A.A. and Kothawale, D.R. (1994) All India Monthly and Seasonal Rainfall Series: 1871-1993. *Theoretical and Applied Climatology*, **49**, 217-224. https://doi.org/10.1007/BF00867461

[2] Ghosh, S., Vittal, H., Sharma, T., Karmakar, S., Kasiviswanathan, K.S., Dhanesh, Y., Sudheer, K.P. and Gunthe, S.S. (2016) Indian Summer Monsoon Rainfall: Implications of Contrasting Trends in the Spatial Variability of Means and Extremes. *PLOS ONE*, **11**, e0158670. https://doi.org/10.1371/journal.pone.0158670

[3] Gadgil, S. and Gadgil, S. (2006) The Indian Monsoon, GDP and Agriculture. *Economic and Political Weekly*, **41**, 4887-4895. http://www.jstor.org/stable/4418949

[4] Sarker, S. (2021) Investigating Topologic and Geometric Properties of Synthetic and Natural River Networks under Changing Climate. Electronic Theses and Dissertations, University of Central Florida, Orlando, 965. https://stars.library.ucf.edu/etd2020/965

[5] Sarker, S., Sarker, T., Leta, O.T., Raihan, S.U., Khan, I. and Ahmed, N. (2023) Understanding the Planform Complexity and Morphodynamic Properties of Brahmaputra River in Bangladesh: Protection and Exploitation of Riparian Areas. *Water*, **15**, Article No. 1384. https://doi.org/10.3390/w15071384

[6] Yuan, G., *et al.* (2022) Analyzing the Critical Locations in Response of Constructed and Planned Dams on the Mekong River Basin for Environmental Integrity. *Environmental Research Communications*, **4**, Article ID: 101001. https://doi.org/10.1088/2515-7620/ac9459

[7] Palmer, T.N., *et al.* (2004) Development of a European Multi-Model Ensemble System for Seasonal to Interannual Prediction (DEMETER). *Bulletin of the American Meteorological Society*, **85**, 853-872. https://doi.org/10.1175/BAMS-85-6-853

[8] Saha, S., *et al.* (2006) The NCEP Climate Forecast System. *Journal of Climate*, **19**, 3483-3517. https://doi.org/10.1175/JCLI3812.1

[9] Saha, S., *et al.* (2014) The NCEP Climate 415 Forecast System Version 2. *Journal of Climate*, **27**, 2185-2208. https://doi.org/10.1175/JCLI-D-12-00823.1

[10] Pillai, P.A., Rao, S.A., Das, R.S., Salunke, K. and Dhakate, A. (2018) Potential Predictability and Actual Skill of Boreal Summer Tropical SST and Indian Summer Monsoon Rainfall in CFSv2-T382: Role of Initial SST and Teleconnections. *Climate Dynamics*, **51**, 493-510. https://doi.org/10.1007/s00382-017-3936-y

[11] Mohanty, U.C., Sinha, P., Mohanty, M.R., Maurya, R.K.S. and Rao, M.N. (2019) A Review on the Monthly and Seasonal Forecast of the Indian Summer Monsoon. *Mausam*, **70**, 425-442. https://doi.org/10.54302/mausam.v70i3.223

[12] Wang, B., Lee, J.Y., Kang, I.S., *et al.* (2009) Advance and Prospectus of Seasonal Prediction: Assessment of the APCC/CliPAS 14-Model Ensemble Retrospective Seasonal Prediction (1980-2004). *Climate Dynamics*, **33**, 93-117. https://doi.org/10.1007/s00382-008-0460-0

[13] Kar, S.C., Acharya, N., Mohanty, U. and Kulkarni, M.A. (2012) Skill of Monthly Rainfall Forecasts over India Using Multi-Model Ensemble Schemes. *International Journal of Climatology*, **32**, 1271-1286. https://doi.org/10.1002/joc.2334

[14] Mohanty, M.R., Sinha, P., Maurya, R.K.S. and Mohanty, U.C. (2019) Moisture Flux Adjustments in RegCM4 for Improved Simulation of Indian Summer Monsoon Precipitation. *Climate Dynamics*, **52**, 7049-7069. https://doi.org/10.1007/s00382-018-4564-x

[15] Chevuturi, A., Turner, A.G., Johnson, S., Weisheimer, A., Shonk, J.K., Stockdale, T.N. and Senan, R. (2021) Forecast Skill of the Indian Monsoon and Its Onset in the ECMWF Seasonal Forecasting System 5 (SEAS5). *Climate Dynamics*, **56**, 2941-2957. https://doi.org/10.1007/s00382-020-05624-5

[16] Pradhan, P.K., Prasanna, V., Lee, D.Y. and Lee, M.I. (2015) El-Niño and Indian Summer Monsoon Rainfall Relationship in Retrospective Seasonal Prediction Runs: Experiments with Coupled Global Climate Models and MMEs. *Meteorology and Atmospheric Physics*, **128**, 97-115. https://doi.org/10.1007/s00703-015-0396-y

[17] Alessandri, A., Borrelli, A., Navarra, A., Arribas, A., Déqué, M., Rogel, P. and Weisheimer, A. (2011) Evaluation of Probabilistic Quality and Value of the ENSEMBLES Multimodel Seasonal Forecasts: Comparison with DEMETER. *Monthly Weather Review*, **139**, 581-607. https://doi.org/10.1175/2010MWR3417.1

[18] Kim, H.M., Webster, P.J., Curry, J.A. and Toma, V.E. (2012) Asian Summer Monsoon Prediction in ECMWF System 4 and NCEP CFSv2 Retrospective Seasonal Forecasts. *Climate Dynamics*, **39**, 2975-2991. https://doi.org/10.1007/s00382-012-1470-5

[19] Mohanty, M.R., Pradhan, M., Maurya, R.K.S., Rao, S.A., Mohanty, U.C. and Landu, K. (2021) Evaluation of State-of-the-Art GCMs in Simulating Indian Summer Monsoon Rainfall. *Meteorology and Atmospheric Physics*, **133**, 1429-1445. https://doi.org/10.1007/s00703-021-00818-w

[20] Gadgil, S., Rajeevan, M. and Nanjundiah, R. (2005) Monsoon Prediction—Why Yet Another Failure? *Current Science*, **88**, 1389-1400.

[21] Wang, B., Xiang, B., Li, J., *et al.* (2015) Rethinking Indian Monsoon Rainfall Prediction in the Context of Recent Global Warming. *Nature Communications*, **6**, Article No. 7154. https://doi.org/10.1038/ncomms8154

[22] Rao, S.A., Pillai, P.A., Pradhan, M. and Srivastava, A. (2019) Seasonal Prediction of Indian Summer Monsoon in India: The Past, the Present and the Future. *Mausam*, **70**, 265-276. https://doi.org/10.54302/mausam.v70i2.171

[23] Madolli, M.J., Himanshu, S.K., Patro, E.R., *et al.* (2022) Past, Present and Future Perspectives of Seasonal Prediction of Indian Summer Monsoon Rainfall: A Review. *Asia-Pacific Journal of Atmospheric Sciences*, **58**, 591-615. https://doi.org/10.1007/s13143-022-00273-6

[24] Goswami, B.N., Venugopal, V., Sengupta, D., Madhusoodanan, M.S. and Xavier, P.K. (2006) Increasing Trend of Extreme Rain Events over India in a Warming Environment. *Science*, **314**, 1442-1445. https://doi.org/10.1126/science.1132027

[25] Rasmusson, E.M. and Carpenter, T.H. (1983) The Relationship between Eastern Equatorial Pacific Sea Surface Temperatures and Rainfall over India and Sri Lanka. *Monthly Weather Review*, **1**, 517-528. https://doi.org/10.1175/1520-0493(1983)111<0517:TRBEEP>2.0.CO;2

[26] Ashok, K., Guan, Z. and Yamagata, T. (2001) Impact of the Indian Ocean Dipole on the Relationship between Indian Monsoon Rainfall and ENSO. *Geophysical Research Letters*, **28**, 4499-4502. https://doi.org/10.1029/2001GL013294

[27] Rao, S.A., Chaudhari, H.S., Pokhrel, S. and Goswami, B.N. (2010) Unusual Central Indian drought of Summer Monsoon 2008: Role of Southern Tropical Indian Ocean Warming. *Journal of Climate*, **23**, 5163-5174.

https://doi.org/10.1175/2010JCLI3257.1

[28] Dash, S.K., Nair, A.A., Kulkarni Makarand, A. and Mohanty, U.C. (2011) Characteristic Changes in the Long and Short Spells of Different Rain Intensities in India. *Theoretical and Applied Climatology*, **105**, 563-570. https://doi.org/10.1007/s00704-011-0416-x

[29] Viswanadhapalli, Y., Dasari, H.P., Dwivedi, S., Madineni, V.R., Langodan, S. and Hoteit, I. (2019) Variability of Monsoon Low-Level Jet and Associated Rainfall over India. *International Journal of Climatology*, **40**, 1067-1089. https://doi.org/10.1002/joc.6256

[30] Goswami, B.N. (1998) Interannual Variations of Indian Summer Monsoon in a GCM: External Conditions versus Internal Feedbacks. *Journal of Climate*, **11**, 501-522. https://doi.org/10.1175/1520-0442(1998)011<0501:IVOISM>2.0.CO;2

[31] Guhathakurta, P. and Rajeevan, M. (2008) Trends in the Rainfall Pattern over India. *International Journal of Climatology*, **28**, 1453-1469. https://doi.org/10.1002/joc.1640

[32] Guhathakurta, P., Sreejith, O.P. and Menon, P.A. (2011) Impact of Climate Change on Extreme Rainfall Events and Flood Risk in India. *Journal of Earth System Science*, **120**, 359-373. https://doi.org/10.1007/s12040-011-0082-5

[33] Chevuturi, A., Turner, A.G., Woolnough, S.J., Martin, G.M. and MacLachlan, C. (2019) Indian Summer Monsoon Onset Forecast Skill in the UK Met Office Initialized Coupled Seasonal Forecasting System (GloSea5-GC2). *Climate Dynamics*, **52**, 6599-6617. https://doi.org/10.1007/s00382-018-4536-1

[34] Kumar, A. and Hoerling, M.P. (1995) Prospects and Limitations of Seasonal Atmospheric GCM Predictions. *Bulletin of the American Meteorological Society*, **76**, 335-345. https://doi.org/10.1175/1520-0477(1995)076<0335:PALOSA>2.0.CO;2

[35] Acharya, N., Chattopadhyay, S., Kulkarni, M.A. and Mohanty, U.C. (2012) A Neurocomputing Approach to Predict Monsoon Rainfall in Monthly Scale Using SST Anomaly as a Predictor. *Acta Geophysica*, **60**, 260-279. https://doi.org/10.2478/s11600-011-0044-y

[36] Wang, B., Lee, J.Y., Kang, I.S., Shukla, J., Kug, J.S., Kumar, A., Schemm, J., Luo, J.J., Yamagata, T. and Park, C.K. (2008) How Accurately Do Coupled Climate Models Predict the Asian-Australian Monsoon Interannual Variability? *Climate Dynamics*, **30**, 605-619. https://doi.org/10.1007/s00382-007-0310-5

[37] Bhaskaran, B. and Mitchell, J.F.B. (1998) Simulated Changes in Southeast Asian Monsoon Precipitation Resulting from Anthropogenic Emissions. *International Journal of Climatology*: *A Journal of the Royal Meteorological Society*, **18**, 1455-1462. https://doi.org/10.1002/(SICI)1097-0088(19981115)18:13<1455::AID-JOC331>3.0.CO;2-D

[38] Jacob, D. and Podzun, R. (1997) Sensitivity Studies with the Regional Climate Model REMO. *Meteorology and Atmospheric Physics*, **63**, 119-129. https://doi.org/10.1007/BF01025368

[39] Ji, Y. and Vernekar, A.D. (1997) Simulation of the Asian Summer Monsoons of 1987 and 1988 with a Regional Model Nested in a Global GCM. *Journal of Climate*, **10**, 1965-1979. https://doi.org/10.1175/1520-0442(1997)010<1965:SOTASM>2.0.CO;2

[40] Bhaskaran, B., Jones, R.G., Murphy, J.M. and Noguer, M. (1996) Simulations of the Indian Summer Monsoon Using a Nested Regional Climate Model: Domain Size Experiments. *Climate Dynamics*, **12**, 573-587. https://doi.org/10.1007/s003820050129

[41] Ratnam, J.V. and Cox, E.A. (2006) Simulation of Monsoon Depressions Using MM5: Sensitivity to Cumulus Parameterization Schemes. *Meteorology and Atmospheric Physics*, **93**, 53-78. https://doi.org/10.1007/s00703-005-0160-9

[42] Dash, S.K., Shekhar, M.S. and Singh, G.P. (2006) Simulation of Indian Summer Monsoon Circulation and Rainfall Using RegCM3. *Theoretical and Applied Climatology*, **86**, 161-172. https://doi.org/10.1007/s00704-006-0204-1

[43] Dobler, A. and Ahrens, B. (2010) Analysis of the Indian Summer Monsoon System in the Regional Climate Model COSMO-CLM. *Journal of Geophysical Research: Atmospheres*, **115**, D16101. https://doi.org/10.1029/2009JD013497

[44] Saeed, S., Müller, W.A., Hagemann, S., Jacob, D., Mujumdar, M. and Krishnan, R. (2011) Precipitation Variability over the South Asian Monsoon Heat Low and Associated Teleconnections. *Geophysical Research Letters*, **38**, L08702. https://doi.org/10.1029/2011GL046984

[45] Srinivas, C.V., Hariprasad, D., Bhaskar Rao, D.V., Anjaneyulu, Y., Baskaran, R. and Venkatraman, B. (2013) Simulation of the Indian Summer Monsoon Regional Climate Using Advanced Research WRF Model. *International Journal of Climatology*, **33**, 1195-1210. https://doi.org/10.1002/joc.3505

[46] Attada, R.A., Parekh, A. and Gnanaseelan, C. (2014) Evolution of Vertical Moist Thermodynamic Structure Associated with the Indian Summer Monsoon in a Regional Climate Model. *Pure and Applied Geophysics*, **171**, 1499-1518. https://doi.org/10.1007/s00024-013-0697-3

[47] Maurya, R.K.S., Sinha, P., Mohanty, M.R. and Mohanty, U.C. (2018) RegCM4 Model Sensitivity to Horizontal Resolution and Domain Size in Simulating the Indian Summer Monsoon. *Atmospheric Research*, **210**, 15-33. https://doi.org/10.1016/j.atmosres.2018.04.010

[48] Maurya, R.K.S., Sinha, P., Mohanty, M.R. and Mohanty, U.C. (2017) Coupling of Community Land Model with RegCM4 for Indian Summer Monsoon Simulation. *Pure and Applied Geophysics*, **174**, 4251-4270. https://doi.org/10.1007/s00024-017-1641-8

[49] Viswanadhapalli, Y., Dasari, H.P., Langodan, S., Challa, V.S. and Hoteit, I. (2017) Climatic Features of the Red Sea from a Regional Assimilative Model. *International Journal of Climatology*, **37**, 2563-2581. https://doi.org/10.1002/joc.4865

[50] Maurya, R.K.S., Mohanty, M.R., Sinha, P. and Mohanty, U.C. (2021) Role of Soil Moisture Initialization in RegCM4.6 for Indian Summer Monsoon Simulation. *Pure and Applied Geophysics*, **178**, 4221-4243. https://doi.org/10.1007/s00024-021-02853-5

[51] Mohanty, M.R. and Mohanty, U.C. (2023) Inter-Comparison of Two Regional Climate Models (RegCM and WRF) in Downscaling CFSv2 for the Seasonal Prediction of Indian Summer Monsoon. *Theoretical and Applied Climatology*, **151**, 99-114. https://doi.org/10.1007/s00704-022-04278-z

[52] Sinha, P., Maurya, R.K.S., Mohanty, M.R. and Mohanty, U.C. (2019) Inter-Comparison and Evaluation of Mixed-Convection Schemes in RegCM4 for Indian Summer Monsoon Simulation. *Atmospheric Research*, **215**, 239-252. https://doi.org/10.1016/j.atmosres.2018.09.002

[53] Dasari, H.P., Srinivas, D., Sabique, L., Karumuri, R.K., Sing, S. and Ibrahim, H. (2020) Atmospheric Conditions and Air Quality Assessment over NEOM, Kingdom of Saudi Arabia. *Atmospheric Environment*, **230**, Article ID: 117489. https://doi.org/10.1016/j.atmosenv.2020.117489

[54] Giorgi, F., Hewitson, B., Christensen, J., Fu, C., Hulme, M., Mearns, L. and Whet-

ton, P. (2001) Regional Climate Simulation-Evaluation and Projections. IPCC WG1 Third Assessment Report.

[55] Christensen, J.H., Hewitson, B., Busuioc, A., Chen, A., Gao, X., Held, I. and Whetton, P. (2007) Chapter 11. Regional Climate Projections. In: Solomon, S., Qin, D., Manning, M., Chen, Z., Marquis, M., Averyt, K.B., Tignor, M. and Miller, H.L., Eds., *Climate Change* 2007: *The Physical Science Basis. Contribution of Working Group I to the Fourth Assessment Report of the Intergovernmental Panel on Climate Change*, Cambridge University Press, Cambridge, 851-853.

[56] Piani, C., Weedon, G.P., Best, M., Gomes, S.M., Viterbo, P., Hagemann, S. and Haerter, J.O. (2010) Statistical Bias Correction of Global Simulated Daily Precipitation and Temperature for the Application of Hydrological Models. *Journal of Hydrology*, **395**, 199-215. https://doi.org/10.1016/j.jhydrol.2010.10.024

[57] Pal, J.S., Giorgi, F., Bi, X., Elguindi, N., Solmon, F., Gao, X. and Steiner, A.L. (2007) Regional Climate Modeling for the Developing World: The ICTP RegCM3 and RegCNET. *Bulletin of the American Meteorological Society*, **88**, 1395-1410. https://doi.org/10.1175/BAMS-88-9-1395

[58] Giorgi, F. (2019) Thirty Years of Regional Climate Modeling: Where Are We and Where Are We Going Next? *Journal of Geophysical Research*: *Atmospheres*, **124**, 5696-5723. https://doi.org/10.1029/2018JD030094

[59] Skamarock, W.C., Klemp, J.B., Dudhia, J., Gill, D.O., Barker, D.M., Duda, M.G., Huang, X.Y., Wang, W. and Powers, J.G. (2008) A Description of the Advanced Research WRF Version 3. NCAR Technical Note NCAR/TN475+STR 113.

[60] Pai, D.S., Rajeevan, M., Sreejith, O.P., Mukhopadhyay, B. and Satbha, N.S. (2014) Development of a New High Spatial Resolution (0.25 × 0.25) Long Period (1901-2010) Daily Gridded Rainfall Data Set over India and Its Comparison with Existing Data Sets over the Region. *Mausam*, **65**, 1-18. https://doi.org/10.54302/mausam.v65i1.851

[61] Hersbach, H., Bell, B., Berrisford, P., *et al.* (2019) The ERA5 Global Reanalysis. *Quarterly Journal of the Royal Meteorological Society*, **146**, 1999-2049. https://doi.org/10.1002/qj.3803

[62] Yanai, M., Esbensen, S. and Chu, J.H. (1973) Determination of Bulk Properties of Tropical Cloud Clusters from Large-Scale Heat and Moisture Budgets. *Journal of Atmospheric Sciences*, **30**, 611-627. https://doi.org/10.1175/1520-0469(1973)030<0611:DOBPOT>2.0.CO;2

[63] Abhik, S., Halder, M., Mukhopadhyay, P., Jiang, X. and Goswami, B.N. (2013) A Possible New Mechanism for Northward Propagation of Boreal Summer Intraseasonal Oscillations Based on TRMM and MERRA Reanalysis. *Climate Dynamics*, **40**, 1611-1624. https://doi.org/10.1007/s00382-012-1425-x

[64] Tao, W.K., Lang, S., Olson, W.S., Meneghini, R., Yang, S., Simpson, J., *et al.* (2001) Retrieved Vertical Profiles of Latent Heat Release Using TRMM Rainfall Products for February 1998. *Journal of Applied Meteorology*, **40**, 957-982. https://doi.org/10.1175/1520-0450(2001)040<0957:RVPOLH>2.0.CO;2

[65] Rogers, R.F., Black, M.L., Chen, S.S. and Black, R.A. (2007) An Evaluation of Microphysics Fields from Mesoscale Model Simulations of Tropical Cyclones. Part I: Comparisons with Observations. *Journal of the Atmospheric Sciences*, **64**, 1811-1834. https://doi.org/10.1175/JAS3932.1

[66] Mukhopadhyay, P., Taraphdar, S., Goswami, B.N. and Krishnakumar, K. (2010) Indian Summer Monsoon Precipitation Climatology in a High-Resolution Regional Climate Model: Impacts of Convective Parameterization on Systematic Biases.

Weather and Forecasting, **25**, 369-387. https://doi.org/10.1175/2009WAF2222320.1

[67] Benedict, J.J., Maloney, E.D., Sobel, A.H., Frierson, D.M. and Donner, L.J. (2013) Tropical Intraseasonal Variability in Version 3 of the GFDL Atmosphere Model. *Journal of Climate*, **26**, 426-449. https://doi.org/10.1175/JCLI-D-12-00103.1

[68] Ling, J., Li, C., Zhou, W., Jia, X. and Zhang, C. (2013) Effect of Boundary Layer Latent Heating on MJO Simulations. *Advances in Atmospheric Sciences*, **30**, 101-115. https://doi.org/10.1007/s00376-012-2031-x

[69] Morwal, S.B., Narkhedkar, S.G., Padmakumari, B., Maheskumar, R.S., DeshPande, C.G. and Kulkarni, J.R. (2017) Intra-Seasonal and Inter-Annual Variability of Bowen Ratio over Rain-Shadow Region of North Peninsular India. *Theoretical and Applied Climatology*, **128**, 835-844. https://doi.org/10.1007/s00704-016-1745-6

[70] Morwal, S.B., Padmakumari, B., Narkhedkar, S.G., Reddy, Y.K., Maheskumar, R.S., Pandithurai, G. and Kulkarni, J.R. (2019) Statistical Characteristics of the Cloud Cells in the Categories of Pre-Convective, Convective-Initiation and Convective-Enhancement in the Contrasting Monsoon Seasons over the Rain-Shadow Region of Peninsular India. *Climate Dynamics*, **53**, 2355-2374. https://doi.org/10.1007/s00382-019-04857-3

[71] Ek, M. and Mahrt, L. (1994) Daytime Evolution of Relative Humidity at the Boundary Layer Top. *Monthly Weather Review*, **122**, 2709-2721. https://doi.org/10.1175/1520-0493(1994)122<2709:DEORHA>2.0.CO;2

[72] Shutts, G.J. and Gray, M.E.B. (1999) Numerical Simulations of Convective Equilibrium under Prescribed Forcing. *Quarterly Journal of the Royal Meteorological Society*, **125**, 2767-2787. https://doi.org/10.1002/qj.49712555921

[73] Sakradzija, M. and Hohenegger, C. (2017) What Determines the Distribution of Shallow Convective Mass Flux through a Cloud Base? *Journal of the Atmospheric Sciences*, **74**, 2615-2632. https://doi.org/10.1175/JAS-D-16-0326.1

[74] Stull, R.B. (1988) An Introduction to Boundary Layer Meteorology. Vol. 13, Springer Science & Business Media, Berlin. https://doi.org/10.1007/978-94-009-3027-8

[75] Garratt, J.R. (1994) The Atmospheric Boundary Layer. *Earth-Science Reviews*, **37**, 89-134. https://doi.org/10.1016/0012-8252(94)90026-4

[76] Gupta, K.S. and Ramachandran, R. (1998) Tropical Atmospheric Boundary Layer. *Proceedings-Indian National Science Academy Part A*, **64**, 267-276.

[77] Santanello Jr., J.A., Friedl, M.A. and Kustas, W.P. (2005) An Empirical Investigation of Convective Planetary Boundary Layer Evolution and Its Relationship with the Land Surface. *Journal of Applied Meteorology*, **44**, 917-932. https://doi.org/10.1175/JAM2240.1

[78] Bianco, L., Djalalova, I.V., King, C.W. and Wilczak, J.M. (2011) Diurnal Evolution and Annual Variability of Boundary-Layer Height and Its Correlation to Other Meteorological Variables in California's Central Valley. *Boundary-Layer Meteorology*, **140**, 491-511. https://doi.org/10.1007/s10546-011-9622-4